Technical Information

Cavitation in Control Valves

3

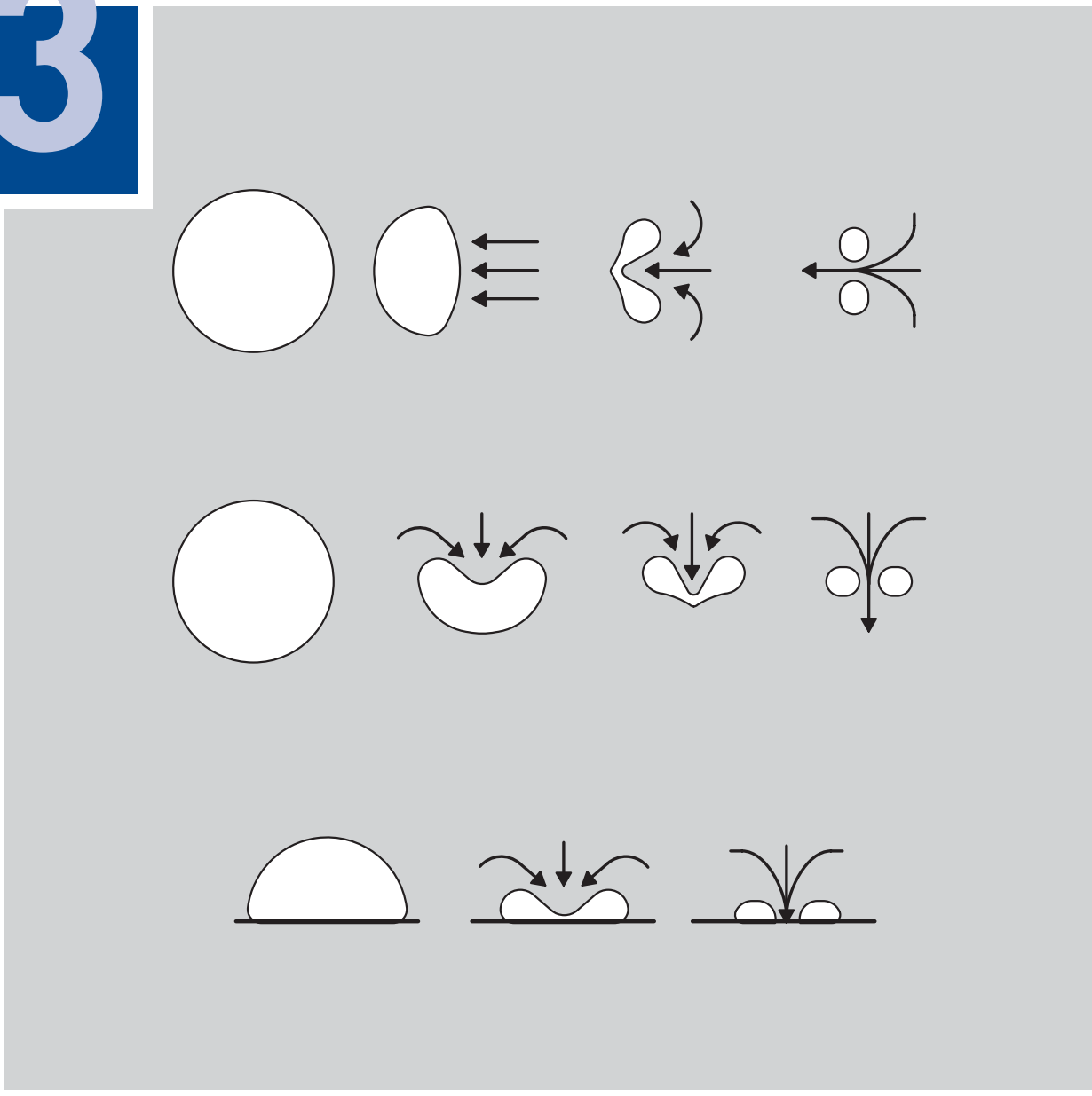

Part 3 Control Valves

Technical Information

Part 1: Fundamentals

Part 2: Self-operated Regulators

Part 3: Control Valves

Part 4: Communication

Part 5: Building Automation

Part 6: Process Automation

Should you have any questions or comments, please contact:

SAMSON AG
V74 / Training
Weismüllerstraße 3
60314 Frankfurt

Phone: +49 69 4009-1467
Fax: +49 69 4009-1716
E-mail: schulung@samson.de
Internet: http://www.samson.de

Cavitation in Control Valves

CONTENTS

SAMSON AG · 03/11

Symbols and units

A	free cross-sectional area at the restriction	[mm^2]
C	bubble volume per volume unit	[-]
c_F	sound velocity in the fluid	[m/s]
C_T	torque coefficient	[-]
d_h	hydraulic diameter	[mm]
E	modulus of elasticity	[N/mm]
E(f)	spectral energy	[W]
f	frequency	[s^{-1}]
F_F	critical pressure ratio factor	[-]
F_L	pressure recovery factor	[-]
G	constant	[Nm]
H	pressure height	[bar]
HV	Vickers hardness	[-]
i	index of throttling step	[-]
k	exponent for the ratio of erosion velocity	[-]
K	compressibility	[m^2/N]
K_C	pressure ratio at incipient cavitation influence on flow rate	[-]
K_R	cavitation resistance	[h/mm^3]
K_v	flow coefficient	[m^3/h]
L_{Wi}	unweighted sound power (inside)	[dB]
M_T	torque	[Nm]
n	number of stages, times or events	[-]
N	amount of substance	[mol]

SAMSON AG · V74/ Dab/Zin

p	pressure	$[N/m^2]$
p_C	critical thermodynamic pressure	[bar]
p_C	pressure in the bubble	$[N/m^2]$
p_G	partial pressure of the gas	$[N/m^2]$
p_{min}	minimum pressure in the control valve	[bar]
p_N	standard pressure	$[N/m^2]$
p_V	vapor pressure	$[N/m^2]$, [bar]
p_1	upstream pressure	[bar]
p_2	downstream pressure	[bar]
Q	flow rate	$[m^3/h]$
r	distance between sound source and observer	[m]
R	nucleus or bubble radius	[m]
R_E	final radius of cavitation bubble	[m]
R_G	gas constant	$[N/mm^2]$
R_k	critical nucleus radius	[m]
R_{max}	maximum radius of cavitation bubble	[mm]
R_m	tensile strength	$[N/mm^2]$
$R_{p\ 0.2}$	yield point at 0.2 % expansion	$[N/mm^2]$
R_0	initial radius of cavitation bubble	[m]
s	distance between the center of the bubble to the boundary	[mm]
t	time	[s]
T_i	temperature in the bubble	[K]
T	ambient temperature	[K]
U	circumference of the restriction	[mm]

U_R	centripetal velocity	[m/s]
UR	ultimative resilience	[N/mm]
V(t)	rate of change in bubble volume	[m/s]
v	kinematic velocity	[m/s]
W	reference deformation	[N/mm^2]
x_F	pressure ratio	[-]
x_{FZ}	valve-specific cavitation coefficient	[-]
y	load of the control valve in percent	[%]
α	capillary constant	[N/m]
ε	expansion	[mm]
ε_B	rupture expansion when yield point is equal to tensile stress	[mm]
η_F	acoustical efficiency factor	[-]
σ_B	rupture strength	[N/mm^2]
φ	opening angle of the butterfly disc	[°]
ν	kinematic viscosity	[mm^2/s]
ρ_F	fluid density	[kg/m^3]

SAMSON AG · V74/ Dab/Zin

Introduction

Cavitation has been a familiar phenomenon for a long time particularly in shipping. In 1917, the British physicist Lord Rayleigh was asked to investigate what caused fast-rotating ship propellers to erode so quickly. He discovered that the effect of cavitation, already proved in experiments by Reynolds in 1894, was the source of the problem. Despite numerous investigations into the subject of cavitation in the years that followed, many of the accompanying effects have still not yet been completely explained. This is no wonder considering the complexity of the process involving the areas of acoustics, hydrodynamics, thermodynamics, optics, plasma physics and chemistry.

Cavitation can be caused in a fluid by energy input. For example, a laser beam creates a plasma in liquids which causes the liquid to evaporate creating a cavity. Ultrasonic waves can be used to induce complex high-frequency alternating compression and rarefaction phases in liquids which cause cavitation. In this way, cavitation effects can be applied usefully for cleaning surfaces, for non-invasive operations in the field of medicine and for breaking down agglomerates in the textile finishing industry. In sewage treatment plants, cavitation is used to break down molecules and bacteria cell walls, break up pollutants and dissolve out minerals from organic material.

Furthermore, cavitation can arise in hydrodynamic flows when the pressure drops. This effect is, however, regarded to be a destructive phenomenon for the most part. In addition to pump rotors, control valves are particularly exposed to this problem since the static pressure at the vena contracta even at moderate operating conditions can reach levels sufficient for cavitation to start occurring in liquids.

The consequences for a control valve as well as for the entire control process vary and are often destructive:

- Loud noise
- Strong vibrations in the affected sections of the plant
- Choked flow caused by vapor formation
- Change of fluid properties
- Erosion of valve components
- Destruction of the control valve
- Plant shutdown

SAMSON AG · V74/ Dob/Zin

Cavitation

Cavitation shall be generally understood as the dynamic process of the formation and implosion of cavities in fluids.Cavitation occurs, for instance, when high flow velocities cause the local hydrostatic pressure to drop to a critical value which roughly corresponds to the vapor pressure of the fluid. This causes small bubbles filled with steam and gases to form. These bubbles finally collapse when they reach the high-pressure areas as they are carried along by the liquid flow. In the final phase of bubble implosion, high pressure peaks are generated inside the bubbles and in their immediate surroundings. These pressure peaks lead to mechanical vibrations, noise and material erosion of surfaces in walled areas. If cavitation is severe, the hydraulic valve coefficients as well as the fluid properties change.

Incipient cavitation

The term 'cavitation' is derived from the Latin verb *cavitare* meaning 'to hollow out', thus referring to the formation of cavities.

To create cavities in fluids, the fluid must first be expanded and then ruptured. Theoretically, fluids can absorb high tensile strengths or negative pressures. Ackeret [1] estimates the negative pressure required to cause cavitation in pure water at 20 °C, based on the minimum of the van der Waals curve, and receives a theoretically possible tensile strength of 10^4 bar which corresponds approximately to the reciprocal compressibility of water.

The tensile strength of the medium is reduced by the disturbance

Inhomogeneities (disturbances) in the quasi-crystalline structure of water, however, reduce the possible tensile strengths by minimum one order of magnitude. In all probability, submicroscopic accumulations of steam or gas molecules are created at these disturbances with the molecules being in an unstable equilibrium with the fluid. In the case of external tensile strengths (negative pressure), these nuclei can exceed a critical diameter and then grow spontaneously as steam is formed.

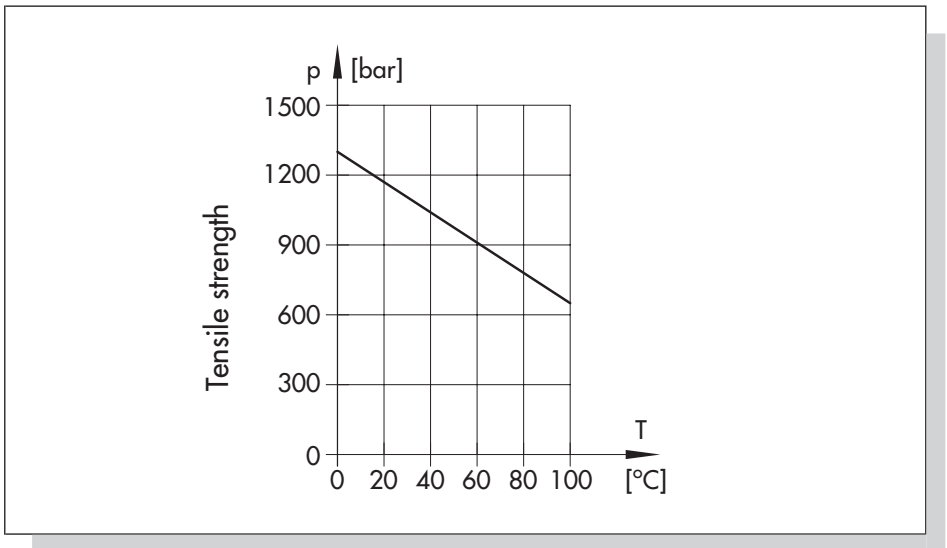

Fig. 1: Theoretical tensile strength values for perfect water

SAMSON AG · V74/ Dob/Zin

By means of statistical examination, Becker and Döring [2] determined the probability for a critical nucleus to occur in dependence of the temperature, resulting in the theoretical tensile strength values for perfect water shown in Fig. 1.

If these values were actually reached for industrial fluids, cavitation in connection with hydraulic systems would not be a matter for discussion. The highest values known until now were derived by measuring centrifugal force as a function of the temperature with extremely pure water. As shown in Fig. 2, the highest value to be achieved was only at 280 bars [3].

Fig. 2 also shows one of the many anomalies of water, i.e. the strong reduction of tensile strength near the freezing point which is caused by the formation of water crystals.

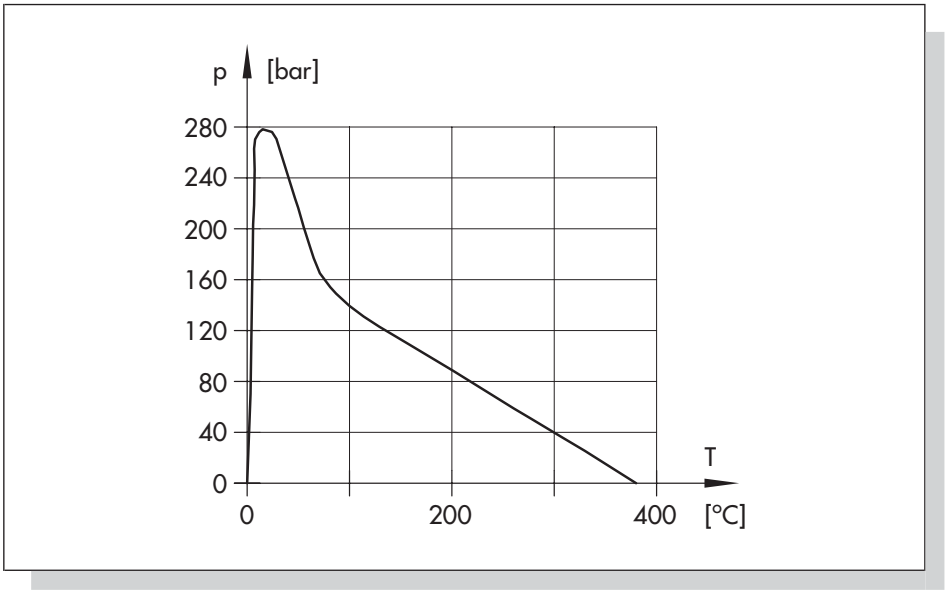

Fig. 2: Tensile strength values derived from measurements for pure water

Cavitation nuclei are decisive for the occurrence of cavitation

The discrepancy between the theoretically and experimentally (under ideal conditions) determined strength values shows that the microscopic bubbles filled with gas and steam (cavitation nuclei), which exist in the fluid and whose existence in water can be explained according to the model by Harvey [4], are a decisive factor in the occurrence of cavitation.

Spherical cavitation nuclei are stable when the fluid pressure p acting on the bubble surface and the partial pressure $2\alpha/ R$ resulting from the surface tension are in equilibrium with the sum of the partial pressures inside the bubble, i.e. the vapor pressure p_V and the pressure of the enclosed gas volume p_G:

$$p_G + p_V = \frac{2\alpha}{R} + p \qquad (1)$$

In this equation, R is the radius of the bubble and α is the capillary constant. If you consider the volume change of the bubble to be isothermal, the following can be derived from the general gas law for spherical nuclei:

$$p_G = \frac{N \cdot R_G \cdot T}{\frac{4}{3} \cdot \pi \cdot R^3} = \frac{G}{R^3} \qquad (2)$$

and with (1)

$$p - p_V = \frac{G}{R^3} - \frac{2\alpha}{R} \qquad (3)$$

with G being proportional to the gas volume contained in the nucleus.

SAMSON AG · V74/ Dob/Zin

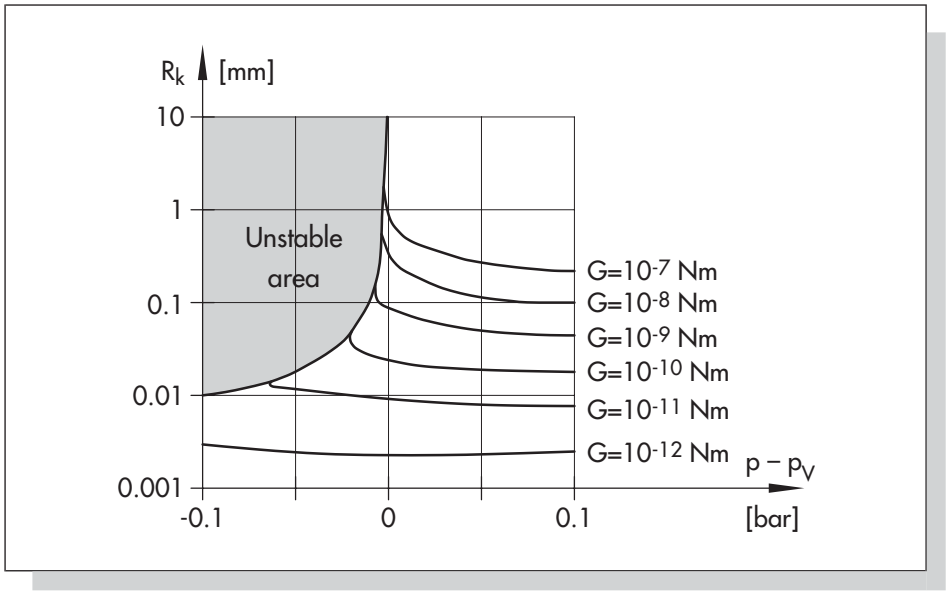

Fig. 3: Critical nucleus radius with varying gas concentrations

The representation $p - p_V = f(R)$ with G as a parameter exemplifies incipient cavitation: (Fig. 3)

When parameters are fixed, at first the radius of the nucleus will increase only slowly as the static pressure decreases. A small change in pressure only results in unlimited bubble growth, i.e. incipient cavitation, after a critical pressure difference has been reached which is mathematically defined by $d(p - p_V)/dR = 0$ and which is derived from:

$$(p - p_V)_{krit} = -\frac{4\alpha}{3 \cdot \sqrt{3}} \cdot \sqrt{\frac{2\alpha}{G}} \qquad (4)$$

Large nuclei, i.e. bubbles with a large G value, start to cavitate first. Their sudden growth accelerates the ambient fluid and reduces the pressure locally. This pressure reduction causes the next smaller bubbles to collapse, which in turn build up a pressure field that causes even smaller bubbles to collapse, and so forth.

Incipient cavitation starts just below vapor pressure

As a result, the critical pressure at which cavitation stops is higher than the critical pressure at incipient cavitation. Lehmann and Young [5] examined the phenomenon of cavitation hysteresis in depth and found that the end of cavitation can be more easily reproduced than incipient cavitation. In particular cases, it therefore depends on the state of the liquid, especially the temperature, spectrum of nuclei, the content of dissolved gases and the surface tension, at which static pressure cavitation begins. Generally, this is just below the vapor pressure. In practice, it is impossible to determine a liquid's spectrum of nuclei in advance for most applications. Therefore, it is common practice in control valve sizing to describe the critical state of the cavitation nuclei at incipient cavitation by means of the vapor pressure of the liquid.

The cavitation coefficient x_{FZ}

In the case of less viscous liquid flows around streamlined bodies, the internal friction compared to the pressure may be frequently neglected. The velocity distribution of these types of flow can be calculated on the basis of the potential theory if the flow conditions are known. The pressure distribution along the body contour is derived from Bernoulli's equation so that a relationship between the minimum pressure p_{min} and the critical pressure can be stated according to equation (4).

Stalling flows occur in control valves

In case of stalling flows as they occur in control valves, the potential theory cannot be used to determine the minimum pressure. Instead, the cavitation coefficient x_{FZ} [6] has proven useful.

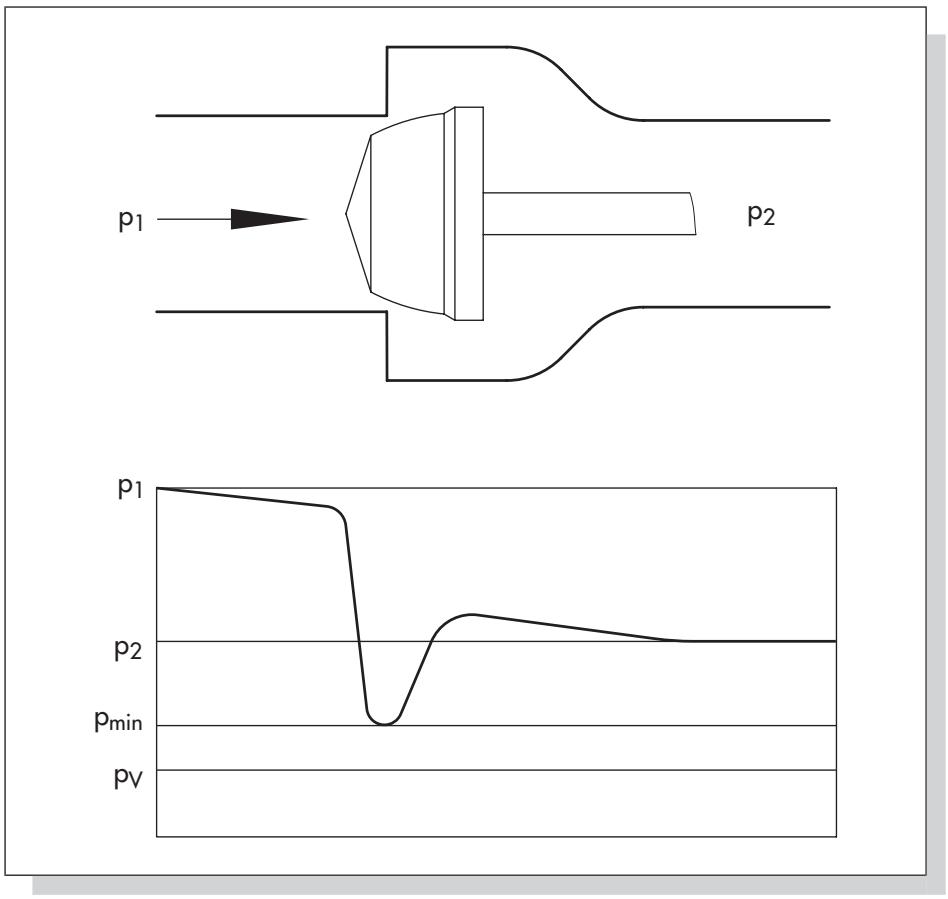

Fig. 4: Distribution of pressure in the valve

It is based on the assumption that, in a control valve, the ratio of the external pressure difference ($p_1 - p_2$) to the internal pressure difference ($p_1 - p_{min}$) for all cavitation-free operating states equals a valve-specific value x_{FZ} (Fig. 4):

$$x_{FZ} = \frac{p_1 - p_2}{p_1 - p_{min}} \qquad (5)$$

Minimum pressure occurs downstream of the restriction

Since the minimum pressure occurs in one of the unsteady vortex cores downstream of the restriction, it cannot be determined by direct measurement.

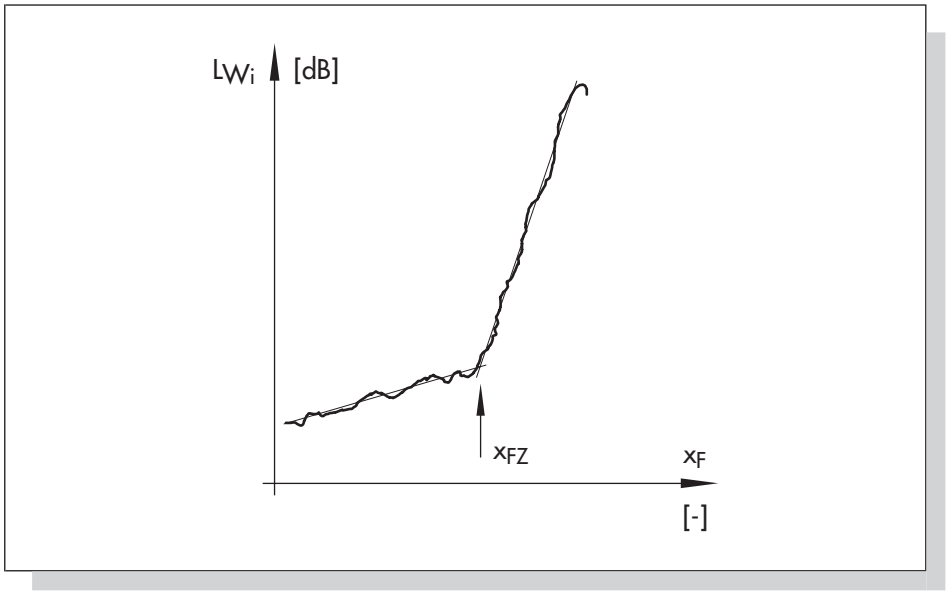

Fig. 5: Determining the cavitation coefficient x_{FZ}

The cavitation coefficient x_{FZ} is determined by noise measurements

It is therefore assumed that the minimum pressure p_{min} equals the vapor pressure p_V of the fluid when cavitation noise begins, thus determining the pressure ratio x_{FZ} as a function of the valve load y by means of noise measurements [7] (Fig. 5).

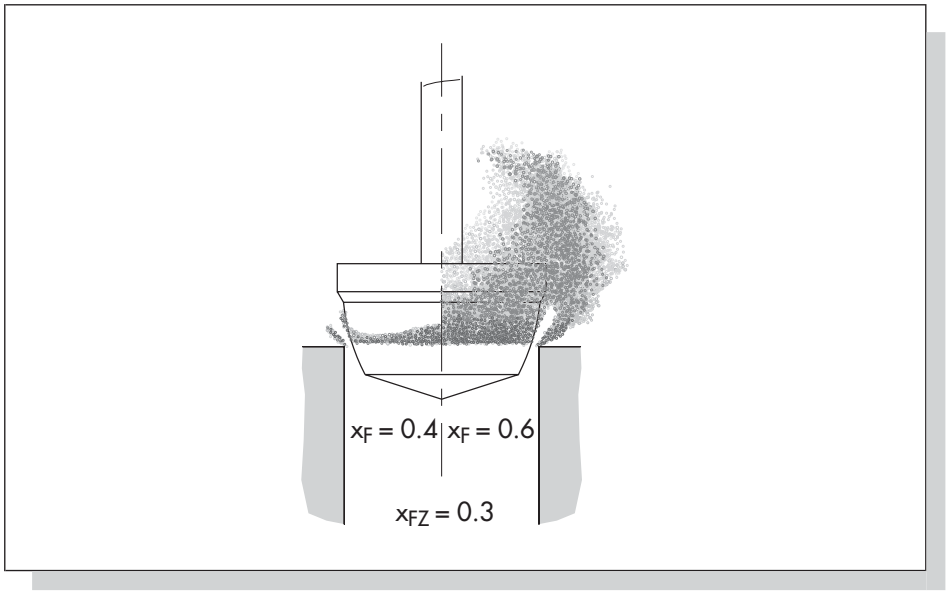

Fig. 6: Formation of cavitation zones with various x_F values

If a valve's x_{FZ} values are known over the entire travel range, it can be determined in advance for all operating pressure ratios

$$x_F = \frac{\Delta p}{p_1 - p_V} \qquad (6)$$

whether cavitation effects are to be expected. In case of an operating pressure ratio $x_F < x_{FZ}$, there is no danger of cavitation occurring; when $x_F \geq x_{FZ}$, a stationary cavitation zone builds up whose expansion is roughly proportional to the difference ($x_F - x_{FZ}$), (Fig. 6).

The operating case $x_F = x_{FZ}$ indicates incipient cavitation

However, since the difference $p_V - p_{crit}$ according to equation (4) is not covered by the operating pressure ratio x_F, these relationships can strictly speaking only be applied to media which conform to the test medium water regarding their nuclei spectrum, surface tension and viscosity. Oldenziel [8] clearly showed this by measuring the pressure ratio x_F at incipient cavitation as a function of the gas content of water (Fig. 7).

The experimental x_{FZ} values should therefore be rounded to full five hundredths to account for the accuracy limits of the process.

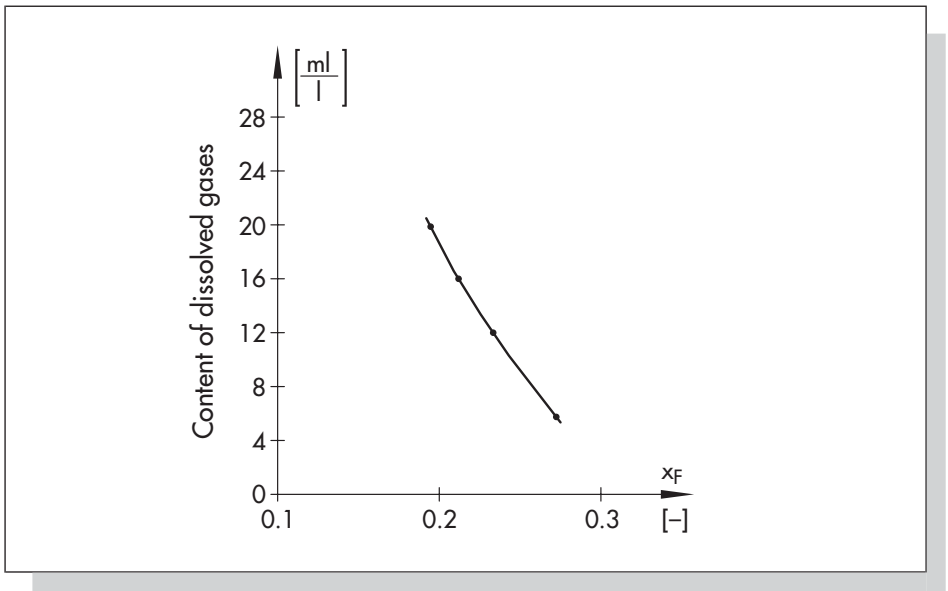

Fig. 7: Relation between the pressure ratio x_F and the gas content

Bubble implosion

Pressure recovery leads to bubble implosion

Due to the pressure recovery inevitable in control valves, the bubbles that are filled with steam and gases reach zones of higher pressure where they implode at high bubble wall velocities. Calculations on the kinetics of the bubble collapse were made as early as 1917 by Rayleigh [9]. While neglecting the surface tension and viscosity, Rayleigh's calculations provide the implosion pressure for a spherical evacuated single bubble

$$p_i = c_F \cdot \rho_F \cdot U_R = c_F \cdot \sqrt{\frac{2}{3} \cdot p_0 \cdot \rho_F \cdot \left(\frac{R_0^{\,3}}{R_E^{\,3}} - 1 \right)} \qquad (7)$$

where c_F and ρ_F are the sound velocity and the fluid density, U_R is the centripetal velocity, p_0 the pressure at indefinite distance, R_0 the initial radius and R_E the final radius of the bubble.

Güth [10] additionally accounts for the gas content of the cavitation bubbles and, assuming an adiabatic compression ($p \cdot V^{\chi}$ = const.), receives the following equation for the maximum implosion pressure.

Maximum implosion pressure of a single bubble

$$p_{i\,max} = p_N \cdot (\chi - 1)^{\frac{\chi}{\chi-1}} \cdot \left(\frac{p_G}{p_N} \right)^{-\frac{1}{\chi-1}} \qquad (8)$$

SAMSON AG · V74/ Dab/Zin

Neglecting the thermal conduction which, however, should be very low due to the short implosion time, for the occurring temperature

$$T_{i\max} = T \cdot (\chi - 1) \cdot \left(\frac{p_G}{p_N} \right) - \frac{1}{\chi} \qquad (9)$$

Maximum occurring temperature

An evaluation of the equations as a function of the ratio partial pressure of the gas inside the bubble p_G to standard pressure p_N, which is a measure for the gas content of the bubble, supplies the following maximum values for T = 293 K and χ = 1.4:

$\frac{p_G}{p_N}$ [-]	$p_{i\max}\left[\frac{N}{mm^2}\right]$	$T_{i\max}$ [K]
0.1	1.3	610
0.05	7.2	990
0.01	405	3140
0.005	2290	5160

Table 1: Maximum values (pressure, temperature) with various gas content

Asymmetric bubble implosion leads to the formation of a microjet

Due to the pressure gradients in the ambient fluid or the influence of rigid boundaries, the cavitation bubbles generally deviate from the spherically symmetric shape. They implode forming a microjet, as high-speed films show and as indicated according to [11] in Fig. 8 for three typical cases. Plesset and Chapman [12] have analyzed the implosion process and found the proportionality

$$v_{jet} \approx \sqrt{\frac{p_\infty - p_V}{\rho_F}} \qquad (10)$$

for the jet velocity

The jet velocity of the microjet reaches up to 100 m/s

Lauterborn [13] used a rotating mirror camera with a frame rate of 900,000 pictures per second to show the formation of a microjet and determined maximum jet velocities between 50 and 100 m/s, which confirmed the values that have been theoretically determined by several authors.

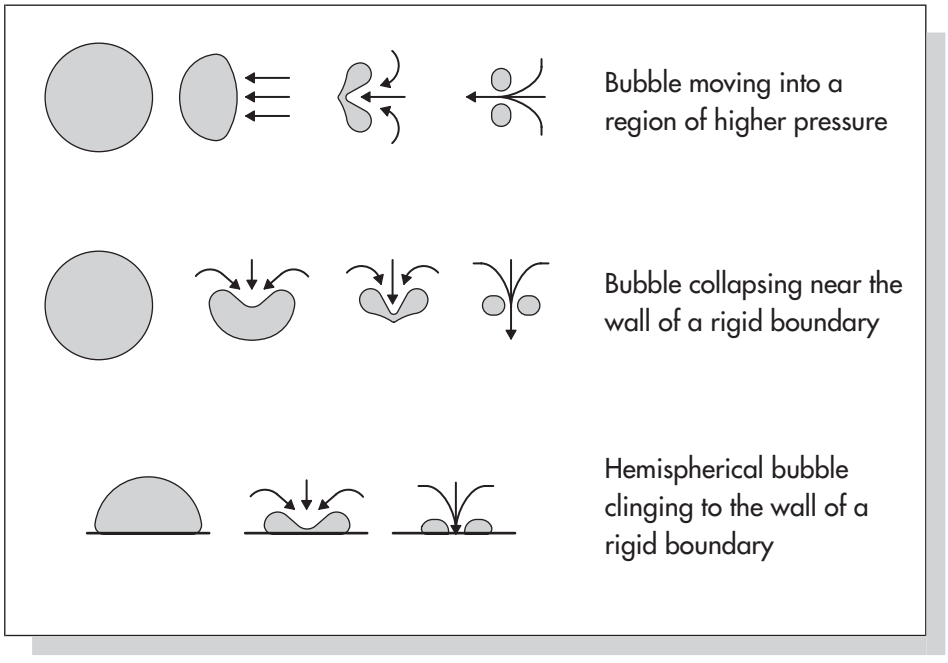

Fig. 8: Diagram illustrating the collapse of a bubble

The pressure created by a fluid jet impact on the wall of a rigid boundary can be easily estimated if the fluid jet is assumed to be a elastic deformable solid.

The application of the principle of conservation momentum results in

$$p_{surge} = \rho_F \cdot c_F \cdot v_{jet} \cdot \frac{\rho_F \cdot c_F}{\rho_W \cdot c_W} + 1$$

and because $w \cdot c_w >> \rho_F \cdot c_F$

$$p_{surge} \approx \rho_F \cdot c_F \cdot v_{jet} \qquad (11)$$

For water ($\rho_F \approx 1000$ kg/m^3, $c_F \approx 1500$ m/s), pressure surges with amplitudes between 750 and 1500 N/mm^2 are reached with the jet velocities mentioned above. Depending on the size of the bubble (radius R), the surge

$$t_{surge} = \frac{2R}{c_F} \qquad (12)$$

lasts between several microseconds and several milliseconds. The effect of one single surge is limited to an area of only a few micrometers in diameter.

The damage to the surface is caused to a considerable extent by the impact of the striking fluid jet and by the shock wave of the imploding bubble. Most probably, the high temperature in the imploding bubble itself is also a key factor.

In his publication [14], Lauterborn showed that the collapsing bubble, which acquires a toroidal shape, becomes unstable and collapses at several locations.

These centers of collapse are the starting point for shock waves which lead to the characteristic toroidal pattern of damage. The extent of damage depends mainly on the dimensionless parameter for distance $\gamma = s/R_{max}$, where s stands for the distance between the center point of the bubble and the boundary at the maximum bubble radius R_{max}. A correlation between liquid jet and pattern of damage arises only when $\gamma < 0.7$, if the bubble is already located at the solid boundary before it collapses. In this case, the jet reaches unobstructed the surface and leaves an impression on the surface [14].

Knapp [15] showed for a stationary cavitation zone according to Fig. 9 that only one out of 30,000 bubbles implodes near the wall, thus having a damaging effect. The number of high-energy surges per cm^2 reaches its maximum at the end of the cavitation zone (Fig. 9).

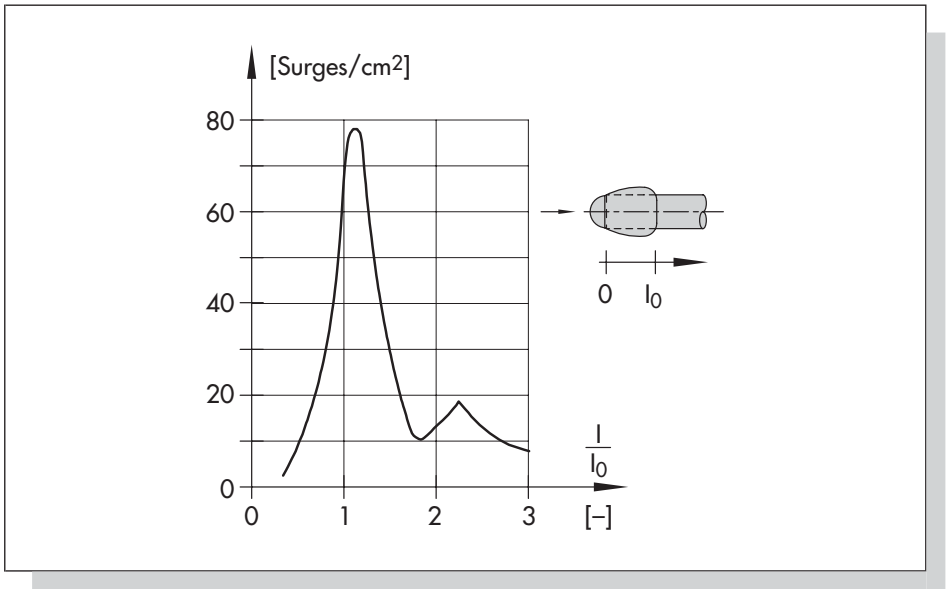

Fig. 9: Number of high-energy surges in a stationary cavitation zone

Cavitation intensity

While the effect of a collapsing bubble can be very well described by theoretical models, the cavitation intensity of a cavitation zone can currently only be described in terms of quality. The following parameters are significant:

- x_{FZ} value of the control valve
- operating pressure ratio x_F
- pressure difference $p_2 - p_V$
- geometry of the control valve downstream of the restriction
- gas contents of the fluid
- fluid viscosity
- surface tension of the fluid
- fluid density

The difference between the pressure in the bubble and the pressure at the site of implosion acts as the driving force when the bubble collapses, see equations (10) and (11). Since the pressure in the bubble is almost equal to the vapor pressure, and the ambient pressure at the site of implosion corresponds approximately to the downstream pressure, the damaging effect of the bubble increases as the difference $p_2 - p_V$ increases. If the difference between downstream pressure and vapor pressure is less than 2 bars, as often is the case in heat supply systems, there is no significant material erosion when non-corrosive media are used. The cavitation zone extends and the number of cavitation bubbles grows as the difference between the pressure ratio x_F and the valve-specific coefficient x_{FZ} for incipient cavitation increase. On the one hand, this leads to an increase in the damaging effect at first. On the other hand, as the difference between x_F and x_{FZ} increases, the duration of the bubble growth phase increases as well. Consequently a larger amount of gases dissolved in the fluid diffuses into the bubble.

The gas diffusion increases as the difference between x_F and x_{FZ} increases

Diffused gas increases the compressibility of the fluid

The diffused gas is transported with the bubble into the cavitation zone and is released when the bubble collapses. As a result, the compressibility K of the fluid increases in the area of the collapse, while the density ρ_F decreases. The sound velocity drops as a consequence

$$c_F = \frac{1}{\sqrt{K \cdot \rho_F}} \qquad (13)$$

The eroding effect decreases as the compressibiliy increases

The result according to equation (11) is a reduction in pressure surge amplitudes causing the eroding effect of the collapsing bubbles to decrease. The cavitation wear under otherwise identical conditions is smaller with supersaturated liquids than with undersaturated liquids due to the same reasons. Besides, an extreme undersaturation causes a drop in the critical pressure at which incipient cavitation occurs to values far below the vapor pressure. This means the incipient cavitation first occurs when the pressure ratio is greater than x_{FZ} and is less intense due to the lack of cavitation nuclei. The bubbles implode all the more energetically, the larger the pressure gradient downstream of the restriction is. At the given operating conditions, the pressure gradient is determined by the geometry of the control valve. The gradient is particularly large when the free jet hits the valve body wall close the restriction. The energy dissipation is low as turbulent mixing has just started in this case, and the pressures close to the wall can reach values similar to the upstream pressure p_1. The driving force for the bubble implosion is then approximately proportional ($p_1 - p_V$) and not as described above ($p_2 - p_V$).

Turbulent mixing causes the pressure to drop

A reduction in viscosity causes, when all other conditions remain the same, an increase in the number and size of the bubbles. Additionally, the kinematic impulse of the microjet at low liquid viscosity is greater than at high viscosity. If laminar flow conditions are assumed due to the small size for the microjet, then the jet velocity is inversely proportional to the viscosity.

SAMSON AG · V74/ Dab/Zin

Then the much quoted exponential correlation between the material erosion Δm and jet velocity v follows

$$\frac{\Delta m_1}{\Delta m_2} = \left(\frac{v_1}{v_2} \right)^k \quad k = 1 \ldots 8 \quad (14)$$

for the distinct influence of operating viscosity on the material erosion

$$\frac{\Delta m_1}{\Delta m_2} = \left(\frac{\nu_2}{\nu_1} \right)^k \quad (15)$$

The erosion rate becomes more rapid as medium density increases

The pressures occurring when the bubble implodes are proportional according to equation (7) to the root of the density. This is why the erosion rate is particularly high when cavitation occurs in mercury or liquefied metals.

The surface tension or capillarity makes the pressure in the bubble increase according to equation (1). Therefore, liquids with smaller surface tension than water cavitate at pressure ratios lower than x_{FZ}. When the conditions are otherwise the same, the size and number of cavitation bubbles increases as the surface tension lessens, while the driving force during bubble implosion is reduced. Technical literature and other sources supplies deviating details about the effect of surface tension on material erosion. It may, however, be assumed that the surface tension influences incipient cavitation considerably, but its effect on material erosion is small when the cavitation is pronounced.

A certain judgement, that experienced engineers are most likely to have, is needed to assess cavitation erosion as the effects of the above described parameters affect and overlap each other.

Cavitation erosion

Cavitation erosion is subdivided into three areas

The material surface, depending on its structure, is deformed, loosened and eventually eroded in particles in various ways due to the frequent strain from the pressure waves created by the microjet occurring when the bubble collapses. Fig. 10 shows how cavitation erosion is generally subdivided into three areas.

- In area I, termed the incubation period, a loss in weight is not yet measurable.
- Area II is characterized by an almost constant erosion rate. Areas and depths of the material erosion increase with time.
- In area III, the surface that is already strongly fractured reduces the probability for an implosion close to the surface as it acts as a kind of protective cushion; the material erodes at a much slower rate.

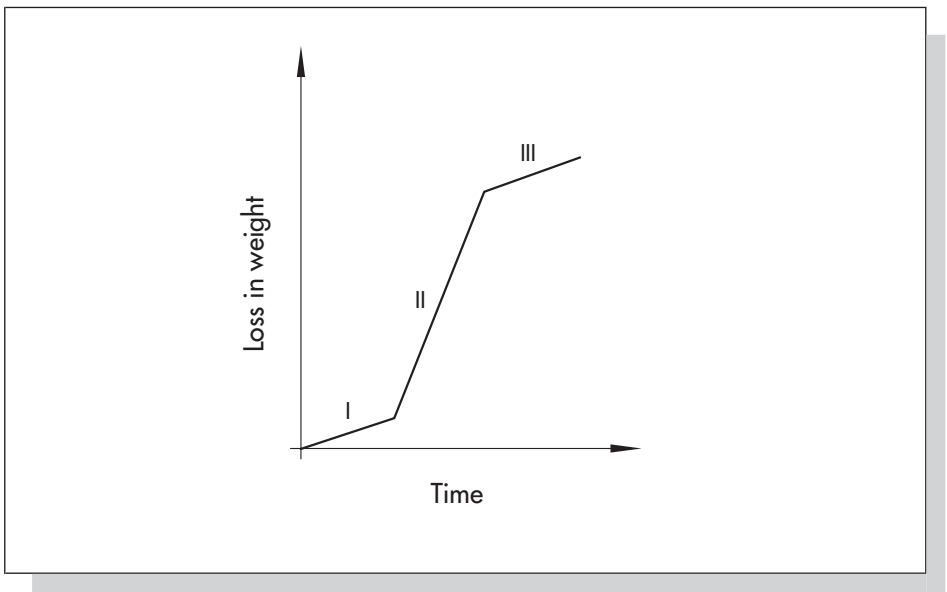

Fig. 10: The course of development of cavitation erosion

SAMSON AG · V74/ Dob/Zin

During the incubation period, the surface of ductile metals first only undergoes elastic deformation and then plastic deformation. Dents and bulges arise. Their number increases as time passes. After the deformability of the material is exceeded at the end of the incubation period, fractures occur and individual particles break off.

The deformation phase does not take place to a great extent with brittle metals due to the high density of dislocation obstacles. As a consequence, internal tensions form that exceed the material strength at the end of the incubation phase. Fractures and ruptures occur that cause a monotonously increasing weight loss. In cast iron, the graphite phase is eroded when the cavitation strain starts, meaning an incubation period can only be mentioned in conjunction with pearlite or ferrite erosion.

After the graphite nodules have been eliminated from spheroidal cast iron, the soft ferrite phase flows into the emptied troughs. The pearlite acts as a supporting frame and slows down surface deformation. The end of the incubation period is reached when the ferrite breaks off at the trough edges after strong deformation and the pearlite material areas break away due to material fatigue.

In cast iron with lamellar graphite, the ferrite is eroded after the incubation time elapses without much plastic deformation because after the graphite has been removed, the contact between the ferrite blocks remains restricted to a few metal bridges which cannot withstand the constant strain.

In ceramic material, microfractures start to appear right from the beginning of the strain without undergoing any noticeable plastic deformation beforehand. As the strain continues, the density of fractures continuously grows. After the incubation time has elapsed, the fractures have spread and joined each other and breakages occur. The incubation in plastics is similar to ductile metals where plastic deformation, formation of cracks and spread of cracks occurs. In crystalline plastics, these structure faults are formed by dislocation, in amorphous plastics by the breaking up of atomic bonds.

In all materials, surface roughness in the area where the bubbles implode leads to a noticeable increase in material erosion since the machining notches help the bubbles to implode energetically and the ridges of the roughly machined surfaces resist the imploding bubbles less than even surfaces would. The influence of the surface roughness must though be observed in conjunction with the microhardness achieved by machining. According to [16], an austenitic steel (EN material no. 1.4919, corresponding to AISI 316 H) with a milled surface has a microhardness $HV_{0.05}$ of 430, whereas it has just 246 with an electrolytically polished surface.

SAMSON AG · V74/ Dob/Zin

Cavitation corrosion

Apart from mechanical strain, corrosive and stress corrosive influences determine the erosion rate of the material. The combination of cavitation erosion and corrosion where the aggressive components can intensify each other is termed cavitation corrosion. The effect of impacting liquid jets intensifies the corrosive attack as the forming top and passivation layers are immediately worn away, causing the high initial corrosion rate typical of bright metal surfaces to be kept as long as the strain lasts.

A beneficial factor for the corrosion process is also the free oxygen which the cavitation bubbles absorb by diffusion, also from undersaturated liquids, while they are growing and which they then release in the cavitation area when they implode.

Additionally, the ions of a corrosive medium are likely to interact with the crystallographic slip steps and fractures of areas that have undergone plastic deformation due to liquid pressure waves. This leads to an accelerated material destruction due to intensified fracture formation or due to fracture spreading.

Cavitation resistance

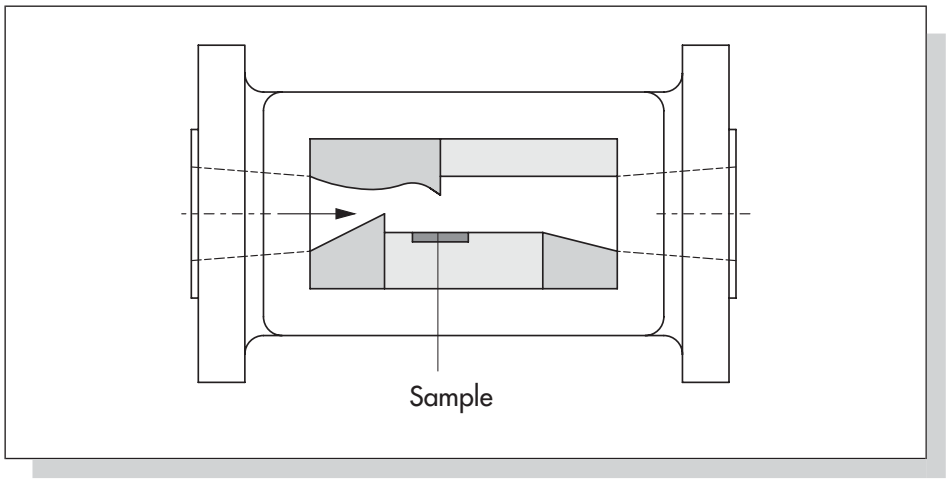

Fig. 11: Cavitation chamber

Magnetostrictive transducers (Fig. 12) as well as cavitation chambers (Fig. 11), electromagnetic, piezoelectric and ultrasonic vibrating instruments are mostly used in laboratories to investigate cavitation resistance of materials. In the magnetostrictive transducer, nickel laminations are excited to vibrate by high-frequency alternating currents.

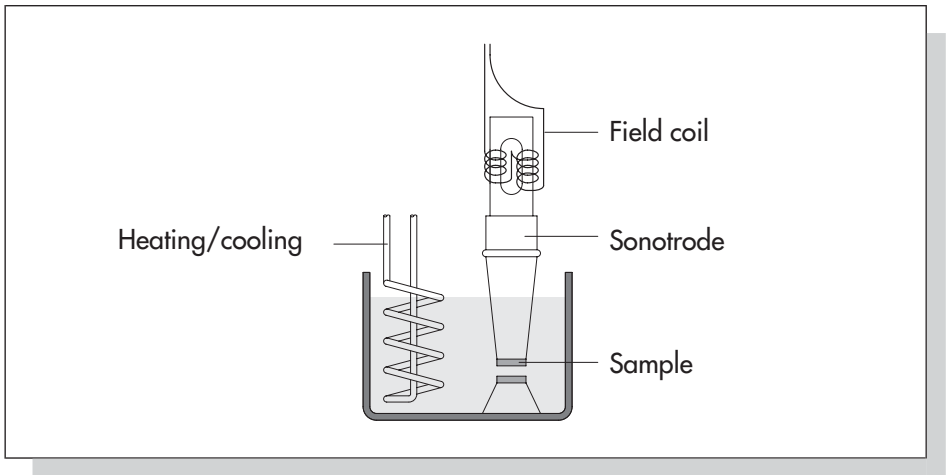

Fig. 12: Magnetostrictive transducer

SAMSON AG · V74/ Dob/Zin

These vibrations are transferred to a coupled sonotrode, which is designed to vibrate in response at the predetermined frequency. The material samples are attached either to the free end of the rod and/or face it at a defined distance.

The liquid surrounding the free end of the rod cannot follow the high-frequency rod oscillations due to its mass inertia, causing liquid cavities in the form of small bubbles to be formed which erode the material when they implode. The test set ups allow cavitation resistance of various materials to be investigated under controlled conditions, making it possible to specify a correlation between the mechanical material characteristics and the erosion rate.

Cavitation resistance K_R

According to the investigations of R. Garcia and F.G. Hammitt [17], the cavitation resistance K_R is proportional to the deformation energy (introduced by Hobbs) up to the point of fracture UR (ultimative resilience – Fig. 13).

$$K_R \approx \sqrt{UR} \qquad (16)$$

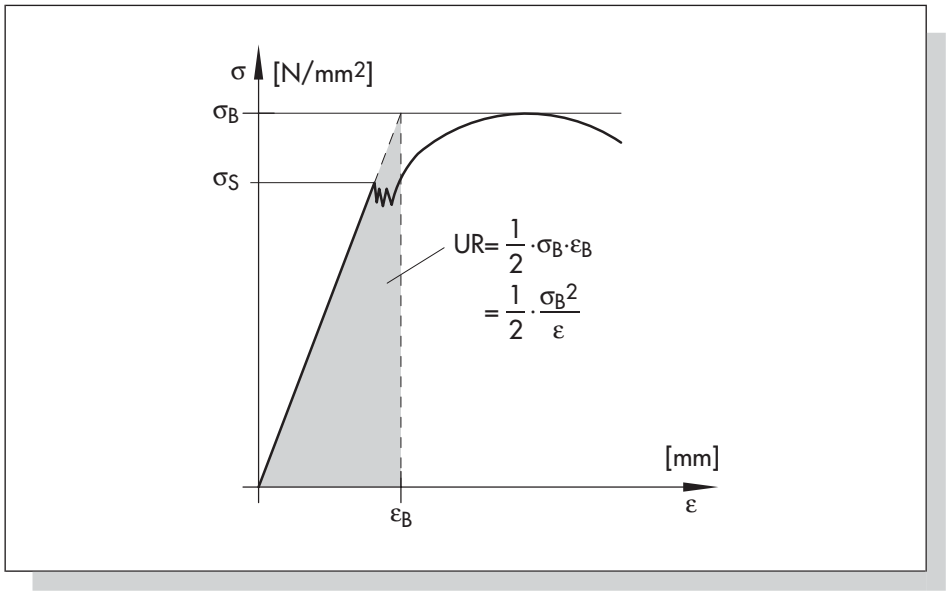

Fig. 13: Material property UR

UR is a combined material property that describes to some extent the energy which could be stored elastically in a material per unit of volume if the yield point could be raised to the level of tensile stress.

Berger [16] describes the cavitation resistance with the relation

$$K_R \approx \frac{R_m^{1.071} \cdot W^{0.125} \cdot HV^{1.971}}{E^{0.562} \cdot R_{p0.2}^{0.618}} \qquad (17)$$

In the equation, E stands for elasticity module, HV for Vickers hardness, R_m for tensile strength and $R_{p\ 0.2}$ for the top yield point or the strength at 0.2% elasticity. The good match of the values calculated according to the equation (17) with values determined in a cavitation chamber (nozzle sample) can be seen in Fig. 14.

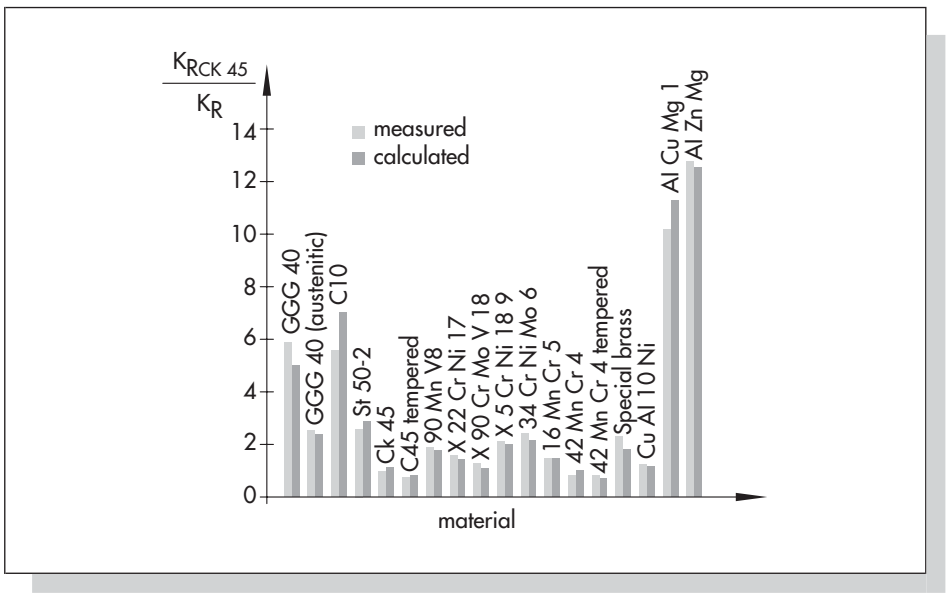

Fig. 14: Cavitation resistance

SAMSON AG · V74/ Dob/Zin

The equations (16) and (17) are only suitable for assessing metals with sufficient elasticity which allow the yield point and deformation energy to be determined in a tensile test.

The applicability of the equations (16) and (17), that were derived from tests with clear water and hydraulic fluid, is still restricted to cases using less corrosive fluids. If cavitation corrosion as described in the section on cavitation corrosion is expected, it is recommendable upon selecting the material to pay attention primarily to the good corrosion resistance and then to take the cavitation resistance into consideration.

Avoiding cavitation

As already explained on page 14, cavitation is avoided when the pressure ratio x_F at the control valve is smaller than the corresponding x_{FZ} value for all operating cases. If the operating pressure ratio x_F is kept small by a clever plant layout, the selection of the control valve decides whether the ratio $x_F < x_{FZ}$ is fulfilled and a cavitation-free flow can be guaranteed.

The x_{FZ} value increases as the opening ratio increases

The x_{FZ} value, which can theoretically be 1 (no pressure recovery) is determined considerably by the Carnot impact loss which is a function of the opening ratios (nominal size cross-section to restriction cross-section). The impact loss and the x_{FZ} value with it, increases as the opening ratio increases, whereas the K_v value drops as the opening ratio increases, which can also be expressed by K_v Control valve/K_{vs} Ball valve.

The x_{FZ} value range of various types of control valves is shown in Fig. 15 as a function of the K_v value of the valve related to the K_{vs} value of a completely open ball valve in the same nominal size.

The bandwidth of the x_{FZ} value range is expressed to a great extent by the hydraulic diameter

$$d_h = 4 \cdot \frac{A}{U} \qquad (18)$$

the shape of the valve plug and seat and the number of pressure reduction stages.

For the free cross-section $A = DN^2 \cdot \pi/4$ of a non-reduced ball valve, the circumference $U = DN \cdot \pi$ and thus the hydraulic diameter is equal to the nominal size DN.

Another expression for the hydraulic diameter is the valve style modifier F_d used in the IEC 60534-2-1 standard [25].

SAMSON AG · V74/ Dob/Zin

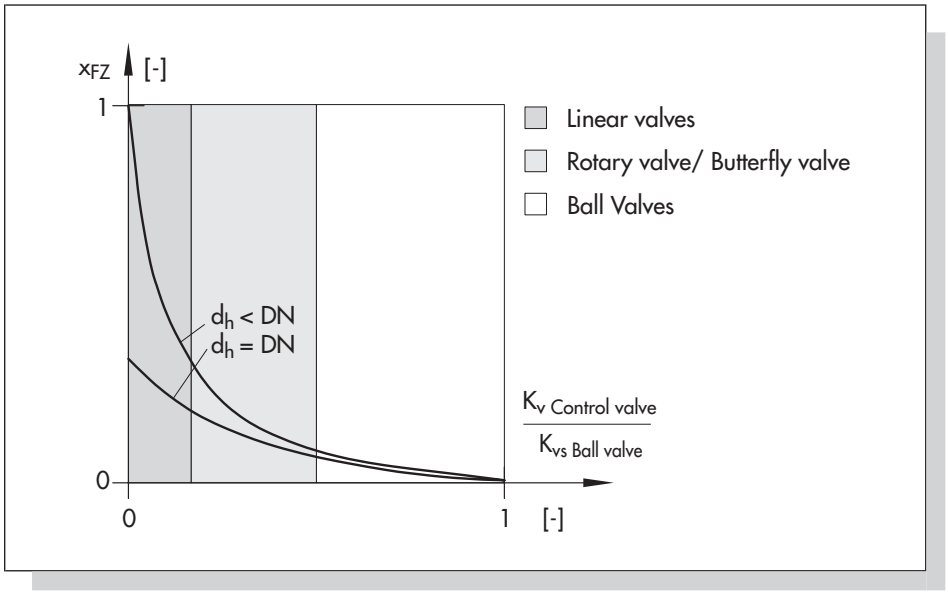

Fig. 15: Control valve operating range without cavitation

In a linear valve with a parabolic plug, the free cross-section is ring-shaped at small loads and the hydraulic radius is just a fraction of the nominal diameter DN. This results in a large surface area of the free jet downstream of the restriction which leads to an intensive impulse exchange with the surrounding medium and causes high pressure losses.

Linear valves allow control without any cavitation even at high pressure ratios

As can be seen in Fig. 15, ball valves only allow the medium to be controlled without cavitation at small pressure ratios. Butterfly valves and rotary plug valves are slightly better, whereas linear valves allow control without any cavitation even at high pressure ratios when the plug is designed accordingly.

Control valves which can be fitted with anti-cavitation trims (Fig. 16) for reducing cavitation and multi-stage axial plugs (Fig. 17) should be given a special mention here.

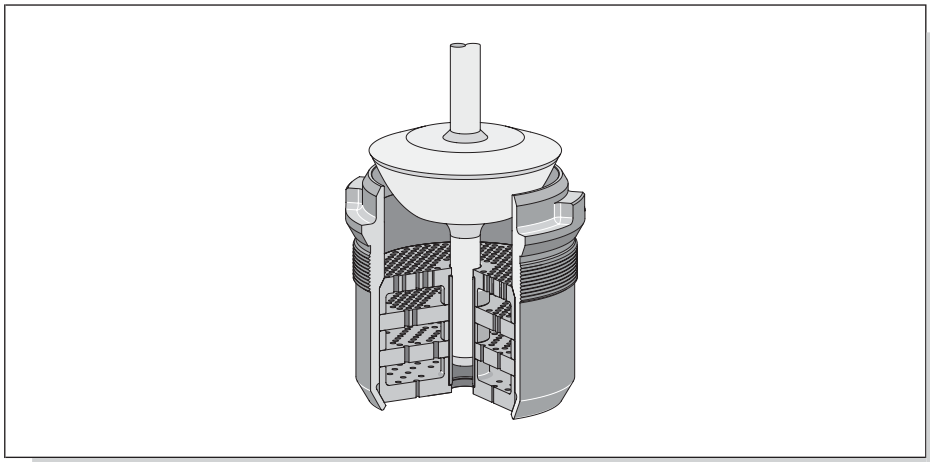

Fig. 16: AC trim system (SAMSON)

The system illustrated in Fig. 16 is a seat and plug trim specially developed for cases where cavitation occurs and designed to be fitted in existing valves. The trim has been optimized in a series of flow simulations and intensive tests. The plug is double guided in the body to prevent mechanical vibrations, and the plug contours have been designed for better flow characteristics. The seat diameter has not been reduced to keep the hydraulic diameter as small as possible. In combination with the special shape of the plug and seat, this is particularly effective. Additionally, a maximum of four attenuation plates can be integrated into the seat to additionally increase the x_{FZ} value at high valve loads [18].

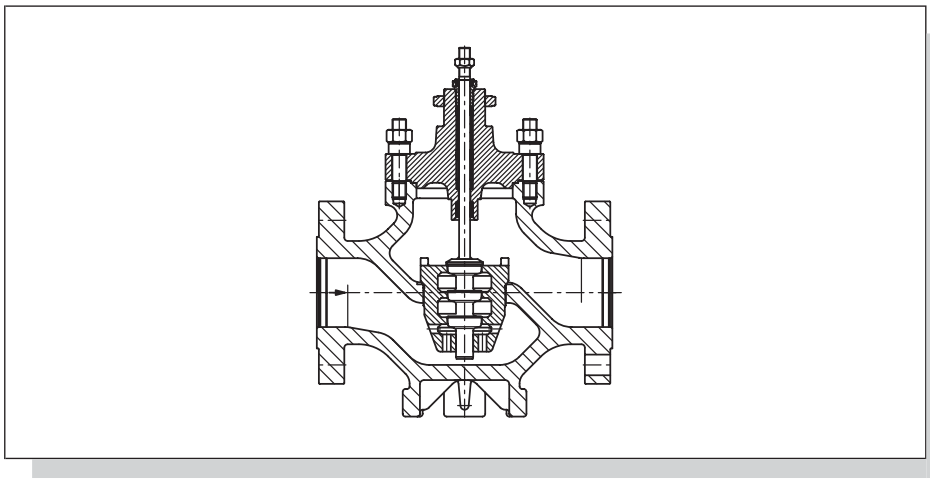

Fig. 17: Multi-stage axial plug (SAMSON Type 3255 Valve)

SAMSON AG · V74/ Dob/Zin

For an initial rough assessment, it is possible to assume that the x_{FZi} values of each individual stage are the same in a valve with a multi-stage plug. Then, the x_{FZ} value is obtained for an n-stage control valve according to

$$x_{FZ} = 1 - (1 - x_{FZi})^n \qquad (19)$$

and for the K_v value ratio of each stage

$$\frac{K_{vi}}{K_{vi+1}} = \sqrt{1 - x_{FZi}} \qquad (20)$$

The K_v value of an n-stage control valve arises from the K_{vi} values of each individual stage according to

$$K_v = \frac{1}{\sqrt{\frac{1}{K_{v1}^2} + \frac{1}{K_{v2}^2} + \ldots + \frac{1}{K_{vn}^2}}} \qquad (21)$$

The number of stages n required to manage an operating pressure ratio x_F free of cavitation is obtained when the x_{FZi} value is known from

$$n = \frac{\lg(1 - x_F)}{\lg(1 - x_{FZi})} \qquad (22)$$

The relationships are easier to understand when looking at Fig. 18. It can be seen that a five-stage valve whose individual stages each have an x_{FZi} value of 0.3 reaches an x_{FZ} value of > 0.8, its K_v value is however just 30% of the K_{vn} value of the last stage. The K_{vn} value corresponds approximately to the K_{vs} value possible in a one-stage valve of the same nominal size. Besides the axial stage plug, the radial stage plugs have proven themselves well in practice (Fig. 19, left).

The x_{FZ} value of the perforated plug (Fig. 19, center) is determined by the opening ratio and the hydraulic radius of the largest hole. The division of holes should be kept to at least three hole diameters to avoid the free jets from joining together before the impulse exchange with the surrounding medium has finished. Just relatively small K_{vs} values (or large opening ratios) are possible especially with equal percentage characteristics. But they lead to high x_{FZ} values as shown in Fig. 15. Valves with perforated cages (Fig. 19, right) function similarly to valves with perforated plugs.

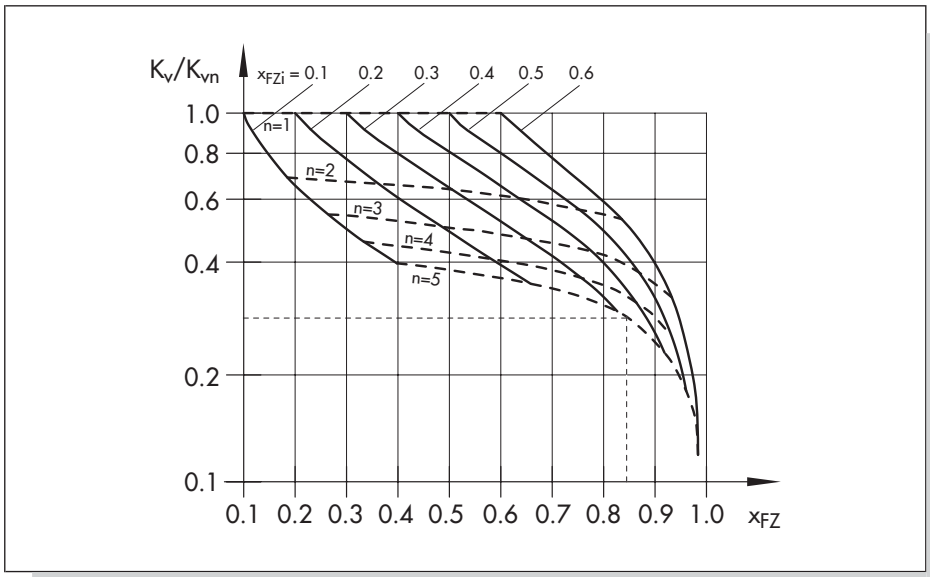

Fig. 18: x_{FZ} values of multi-stage valves

A special design (deviations, restriction cascades) of the ducts allows the countermeasures which increase the x_{FZ} value, for example, high opening ratio, small hydraulic radius and multi-stage throttling, to be combined in one valve. High x_{FZ} values (i.e. low pressure recovery), on the one hand, require large opening ratios, and thus relatively small K_v values. Large K_v values related to the nominal size, on the other hand, always lead to relatively small x_{FZ} values. The x_{FZ} values are listed in the data sheets of control valve manufacturers. Specifications that are outside of the value range shown in Fig. 15 should be viewed critically though.

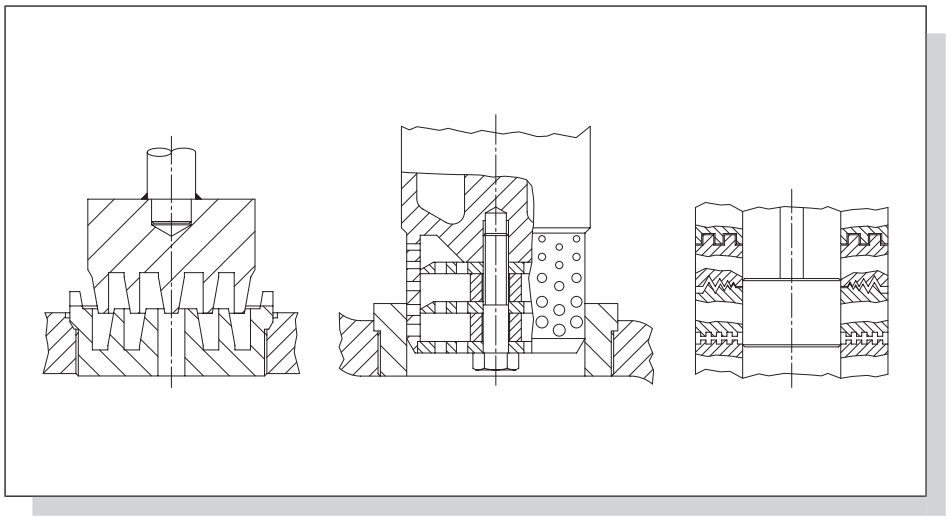

Fig. 19: Plug designs

Operation with cavitation

Since x_{FZ} values necessary for cavitation-free operation cannot always be achieved, or the control valves are too susceptible to dirt or too expensive, making their use uneconomical, valves are often operated in conditions where cavitation occurs. A troublefree operation with a satisfactory service life can be guaranteed though if the effects of cavitation are taken into consideration on sizing and selecting the valve. To ensure that the valve body walls are outside the area at risk of erosion, a larger valve should be selected than required by the valve sizing simply based on the seat diameter. To achieve this, the nominal diameter should be selected to ensure that a certain outlet velocity is not exceeded. It can then be assumed that the cavitation zones will not reach up to the valve walls, and that the bubbles implode without any harm and with little effect (apart from noise).

The following table helps to show whether erosion damage due to cavitation is to be expected. This is the case when $x_F > x_{Fcrit,cav}$ as well as when p_1-$p_2 > \Delta p_{crit,cav}$ [18]. Additionally, a nominal valve size should be selected to ensure that the outlet velocity does not exceed 4 m/s.

Valve design	$x_{Fcrit,cav}$ [-]	$\Delta p_{crit,cav}$ [bar]
Single-stage linear valves	0,7	15
Single-stage linear valves with stellited or hardened trim	0,7	25
3-stage linear valves	1,0	100
5-stage linear valves	1,0	200
Rotary plug valves	0,4	10
Butterfly and ball valves	0,25	5

Table 2: Limit values for preventing cavitation erosion

SAMSON AG · V74/ Dob/Zin

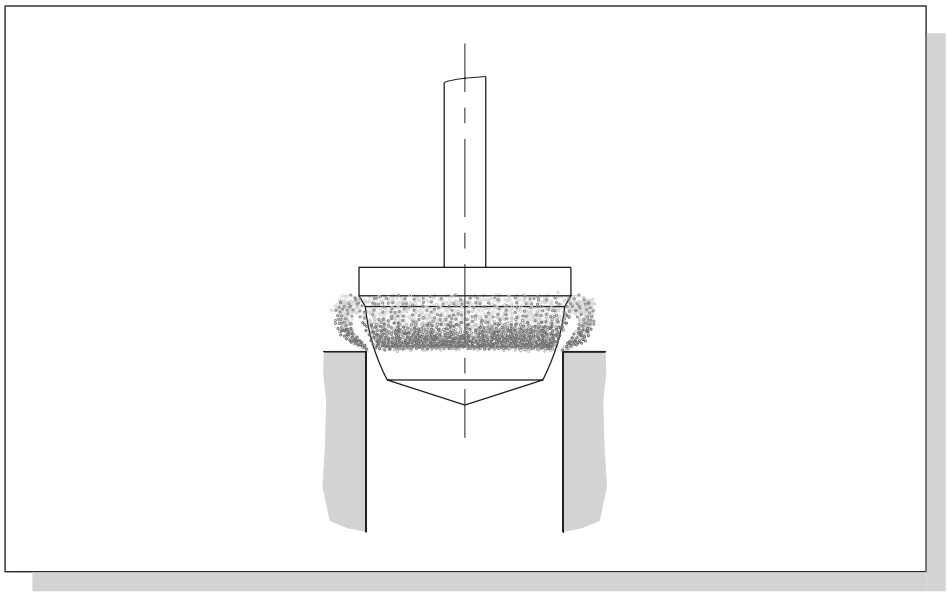

Fig. 20: Areas of a parabolic plug at risk from erosion

The sealing slope and plug surface of paraboloic plugs are particulary at risk from erosion

The sealing slope and plug surface of parabolic plugs are particularly at risk from erosion (Fig. 20).The area around the sealing edge should be given a Stellite facing. A hard facing of the whole surface is recommended when the cavitation intensity increases.

The diverted jet prevents the V-port plug from being eroded

V-port plugs are exposed less to cavitation attacks than parabolic plugs under the same operating conditions. Due to the diverted jet (Fig. 21), the cavitation zones do not stick to the plug surface, meaning the cavitation bubbles implode almost without any effect.

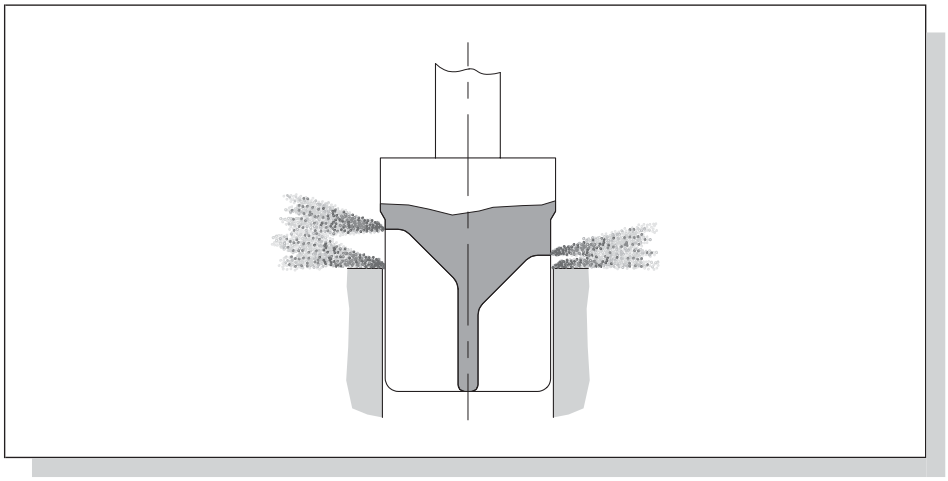

Fig. 21: Diverted jet occurring with a V-port plug

A medium flowing in the reverse direction increases the risk of erosion

The valve seat is not exposed to the cavitation attack when the medium flows against the closing direction. However, if the medium flows in the reverse direction to protect the valve body walls and plug facing (risk of pressure surge waves), the seat and plug surface are then particularly at risk from erosion. A satisfactory service life can only be achieved in this case by using highly resistant materials.

A rising differential pressure can cause the body floor to erode

The perforated plug (Fig. 22) is better suited for medium flow in the reverse direction. A steep pressure gradient that makes the cavitation bubbles implode forms in the center of the plug, i.e. in sufficient distance away from the surface due to the collision of the partial flows. However, the cavitation zone moves out of the plug when the differential pressure rises, causing the body floor to erode. The above mentioned pressure ratios and differential pressures should only be used as a reference for identifying the cavitation intensity. The limits can be considerably reduced as a result of cavitation corrosion, especially when corrosive fluids are used.

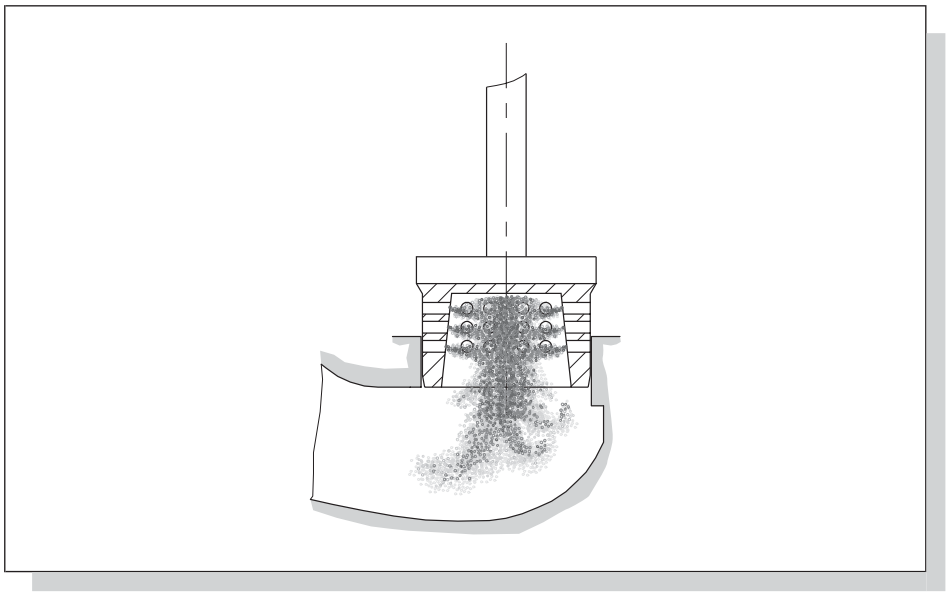

Fig. 22: Cavitation zone with a perforated plug

SAMSON AG · V74/ Dob/Zin

Influence on the hydraulic characteristics

Cavitation changes the density and compressibility of a medium

The continuity of the fluid phase is interrupted when cavitation occurs and the dynamic interaction between flow and its restriction is affected. Additionally, cavitation makes the compressibility of the fluid increase locally and in this way reduces the sound velocity (equation 13). The density of the fluid, too, is drastically reduced by the bubble volume in the area of the restriction as the pressure ratio rises.

These effects limit the flow rate in control valves (choked flow) if a certain differential pressure (Δp_{max}) is exceeded as shown in Fig. 23.

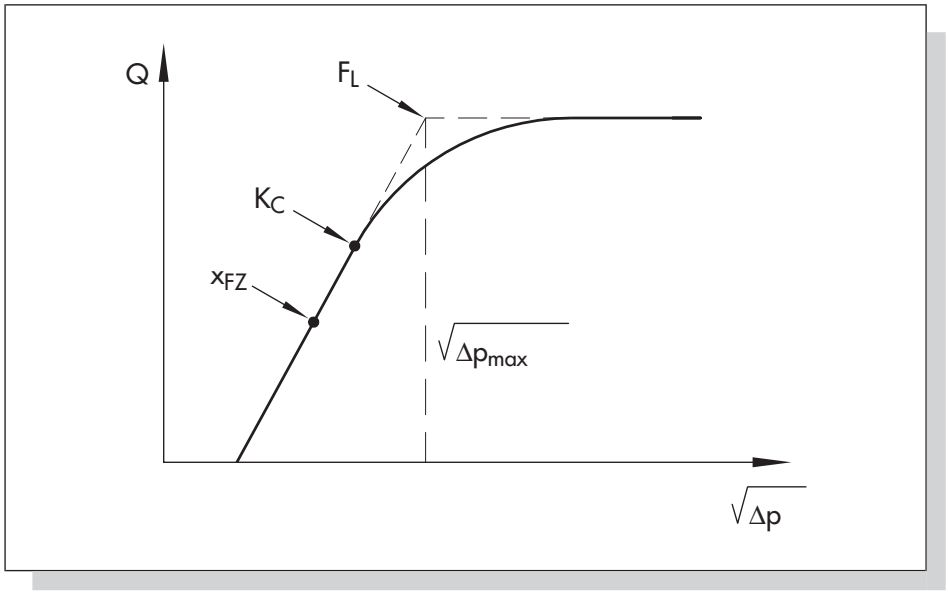

Fig. 23: The valve-specific factor F_L

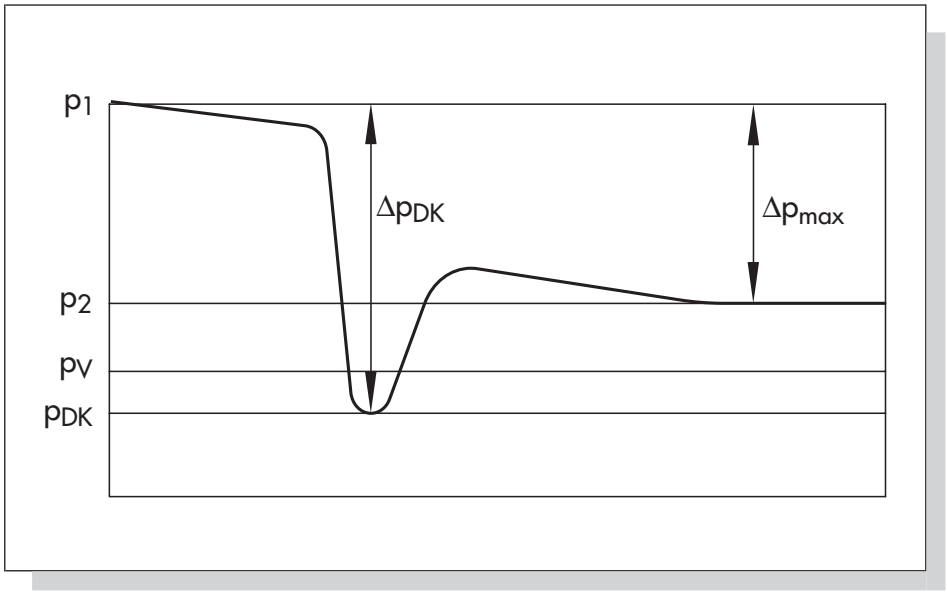

Fig. 24: The critical pressure p_{DK}

The critical pressure is below vapor pressure

The critical pressure p_{DK} is reached at the vena contracta at the differential pressure Δp_{max}, which is below the vapor pressure according to measurements by Stiles [19] (Fig. 24).

Stiles found the relationship shown in Fig. 25 for the ratio between critical pressure at the vena contracta and the vapor pressure

$$F_F = \frac{p_{DK}}{p_V} \qquad (23)$$

from measurements using Frigen 12, which can also be approached using the following equation:

$$F_F = 0.96 - 0.28\sqrt{\frac{p_V}{p_C}} \qquad (24)$$

SAMSON AG · V74/ Dab/Zin

F_L: the factor for pressure recovery

Baumann [20] introduced the valve-specific factor F_L for the ratio between the smallest differential pressure across the valve at which the choked flow starts, Δp_{max} and the critical differential pressure at the vena contracta, Δp_{DK}.

$$F_L^2 = \frac{\Delta p_{max}}{\Delta p_{DK}} \qquad (25)$$

F_L value is the pressure recovery factor. It is determined from a flow rate measurement as in Fig. 23. In this measurement, the upstream pressure is kept constant and the downstream pressure is reduced until choked flow starts. A detailed description of the procedure is specified in IEC 60534, Part 3.

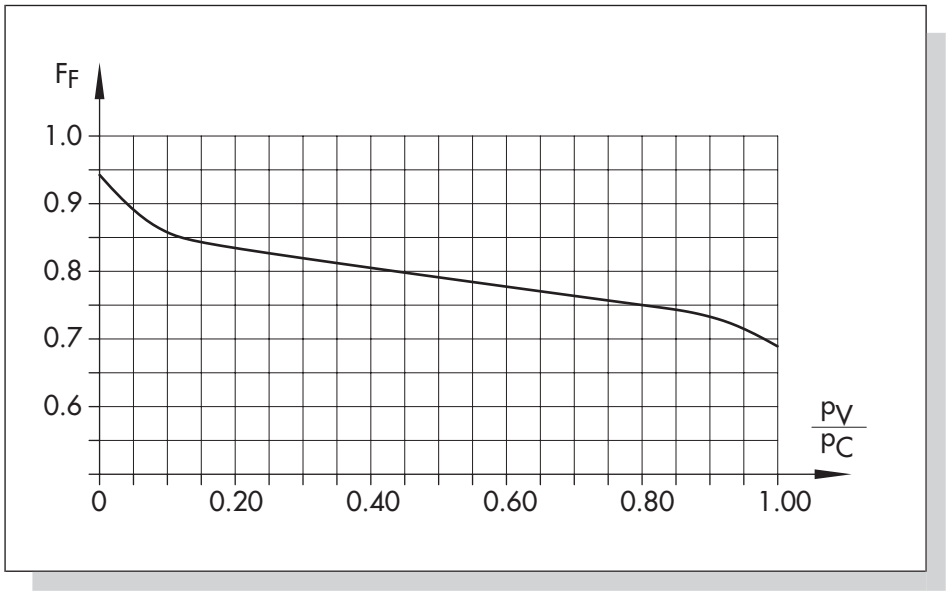

Fig. 25: F_F factor used to determine the critical pressure ratio

The maximum value for differential pressure at which the flow rate is achieved due to cavitation is obtained with the F_L value and equation (23).

$$\Delta p_{max} = F_L^2 (p_1 - F_F \cdot p_V) \qquad (26)$$

The first deviation in flow rate from the general measurement equation

$$Q = K_v \cdot \sqrt{\Delta p \cdot \frac{\rho}{\rho_0}} \qquad (27)$$

is indicated by the pressure ratio.

$$K_C = \frac{\Delta p}{p_1 - p_V} \qquad (28)$$

The K_c value is often referred to as the incipient cavitation index. Yet, incipient cavitation already occurs, as shown in Fig. 23, at the much smaller pressure ratio x_{FZ}. If both coefficients are confused with another, it causes serious mistakes in the assessment of the pressure recovery, the cavitation intensity and noise emission.

The distribution of pressure on the surface of the closure member is also changed by the change in flow pattern due to cavitation.

SAMSON AG · V74/ Dab/Zin

Therefore, the hydraulic torque in butterfly valves, which is calculated with cavitation-free flow according to

$$M_T = C_T \cdot D^3 \cdot H \qquad (29)$$

Hydraulic torque with cavitation-free flow

and works in the closing direction, struggles against a limit value as the pressure ratio grows. In equation (29), D is the disc diameter, C_T the torque coefficient dependent on the opening angle φ, and H the static differential pressure $p_1 - p_2$ across the butterfly valve, increased by the impact pressure of the flow velocity v:

$$H = p + \frac{\rho_F}{2} v^2 \qquad (30)$$

In Fig. 26, the torque for an opening angle φ of 60° is shown as a function of the pressure ratio x_F at constant upstream pressure.

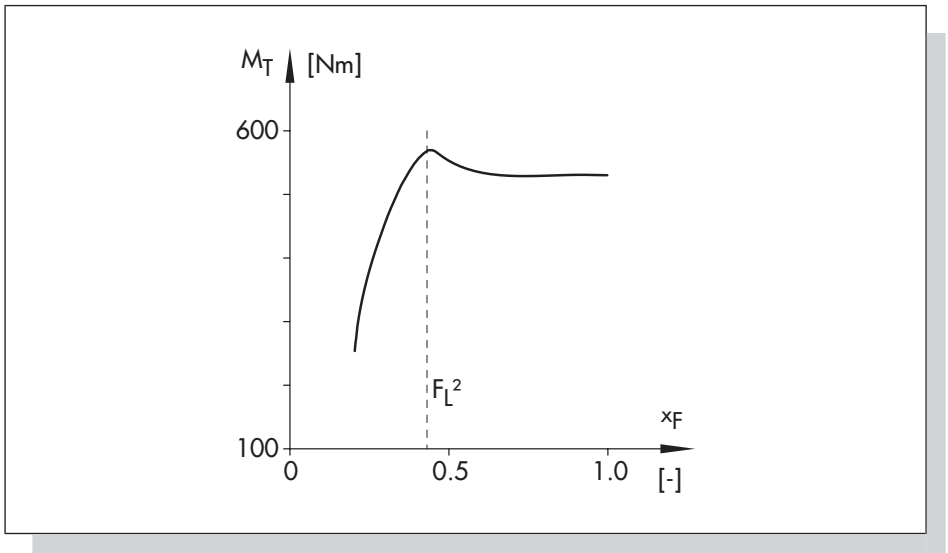

Fig. 26: Course of torque in a butterfly valve

Torque reaches its maximum at choked flow

The torque reaches its maximum at approximately the same differential pressure at which also the choked flow occurs (equation 26). As the pressure ratio (or Δp) further increases, the torque drops slightly at first and then reaches a limit value irrespective of the differential pressure.

When the limit value is reached, the cavitation zone stretches over the whole downstream pressure side, causing the pressure distribution on the inlet side to be approximately constant with the vapor pressure p_V irrelevant of how the pressure ratio increases.

The flow forces around the plug change due to cavitation even in linear valves. However, this change in force is insignificant, except in self-operated regulators where the plug forces must be carefully balanced out by means of pressure balancing.

SAMSON AG · V74/ Dab/Zin

Changes in fluid properties

Not just the surface of the hydraulic components, but even the fluid itself, is exposed to extreme loads when gas-filled cavitation bubbles implode.

The microdiesel effect leads to an accelerated aging of hydraulic fluids

For example, when bubbles implode in hydraulic fluids, temperatures can occur that are sufficient under certain circumstances to ignite bubbles containing air and oil vapor. This process, which is called the microdiesel effect, leads to an accelerated ageing of hydraulic fluids. Cavitation increases the free gas content in the fluid: parts of the gas dissolved in the fluid diffuse into the cavitation bubbles during the growth phase.

The gas parts are released when the bubbles implode and locally increase the compressibility of the fluid. This is accompanied by a reduction in sound velocity, meaning pressure surge and sound propagation calculations in pipelines where cavitation occurs is made more difficult. Fig. 27 shows the sound velocity in water as a function of the bubble concentration according to [21].

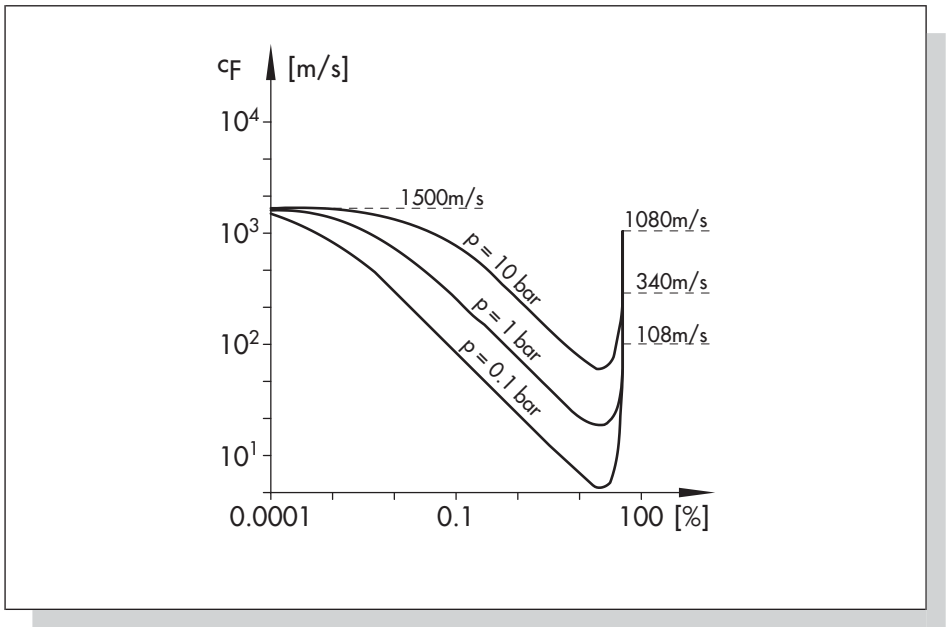

Fig. 27: Sound velocity as a function of the bubble concentration

If oxygen is also released by the cavitation process, the oxidizing effect of the fluid increases. The contamination of the medium caused by cavitation-induced material erosion should not be underestimated in closed circuits.

SAMSON AG · V74/ Dob/Zin

Cavitation noise

The pressure peaks induced by the bubble implosions cause material erosion as well as a loud typical noise. The theoretical approaches to explain how noise develops are based on individual bubbles which implode concentrically in an infinitely expanded fluid and without affecting each other. The cavitation bubble can then be regarded as an isotropic radiator of zero order (monopole source) which creates in the far field the sound pressure

Cavitation bubbles act as an isotropic radiator of zero order

$$p(r,t) = \frac{\rho_F}{4\pi r} \cdot \frac{d^2}{dt^2} \cdot V(t) \cdot \left(t - \frac{r}{c_F} \right) \quad (31)$$

In the equation, V(t) is the rate of change in bubble volume which can be determined approximately using the Rayleigh-Plesset differential equation, and r is the distance between the sound source and the point of observation. The spectral distribution of the energy E(f) of the noise created by a bubble is obtained from the squared Fourier transform of the pressure over time in the far field

$$E(f) = \left(\int_{-\infty}^{+\infty} p(t) \cdot e^{-2\pi i f t} dt \right)^2 \quad (32)$$

while neglecting the retarded time $\left(t - \frac{r}{c_f} \right)$

$$E(f) = \left(\frac{\rho \cdot \pi}{r} \right)^2 \cdot f^4 \cdot \left(\int_{-\infty}^{+\infty} V(t) \cdot e^{-2\pi i f t} dt \right)^2 \quad (33)$$

The spectral energy rises at first with the frequency f raised to the power of four and reaches a maximum at a frequency whose the inverse ratio is approximately the same as the collapsing time of the cavitation bubble. As a consequence of the collapsing time being directly proportional to the bubble radius, the maximum noise is shifted to lower frequencies as the bubble radius increases. At frequencies above the maximum, the spectral energy decreases at $f^{-2/5}$.

If the bubble collapses are observed as random events not connected with one another, whose frequency follows a Poisson distribution, it is possible to derive the total spectral sound energy $E_{total}(f)$ from the spectral energy of individual events E(f) and a mean number of bubble collapses per unit of time n.

$$E_{total}(f) = n \cdot E(f) \qquad (34)$$

Observations of individual bubbles only apply to incipient cavitation

These theoretical considerations made for individual bubbles apply approximately when cavitation just starts. As the cavitation progresses, distinctive cavitation zones form in which the effects of each individual bubble overlap each other, and the contribution of each bubble to the entire noise depends on the history of the neighboring bubble.

More extensive investigations therefore observe the cavitating fluid as a quasi-continuum of density

$$\rho = \frac{\rho_F}{(1+C)} \qquad (35)$$

In the equation, C is the total volume of all bubbles per volume unit. Lyamshev [22] discovered on this basis that the sound intensity of a cavitation zone equals the flow velocity raised to the power of four, or is proportional to the square of the differential pressure.

The theoretical approaches were extended and refined by various authors. Despite this, no one has yet successfully described the exceptionally complex correlations in the cavitation zone downstream of a control valve for various media and pressure ratios.

The equations according to VDMA are based on empirical data

Therefore, the currently valid equations as per the German directive VDMA 24422 to predict noise emission of cavitating flows of control valves are not based on hydrodynamic and thermodynamic models, but instead describe the course of internal sound power level on the basis of measurements related to x_F, z, ρ_F and Δp.

In this case, neither the influence of surface tension nor viscosity nor the influence of the gas contents are taken into account. The influence of the density and the differential pressure important for the course of the bubble implosion

$$p_2 - p_V = \frac{1 - x_F}{x_F} \cdot \Delta p \qquad (36)$$

are also only reproduced inexactly in the empirical VDMA equations which are based mainly on measurements with cold water ($p_V \approx 0$ bar, $\rho_F \approx 1000$ kg/m^3). The VDMA calculation methods [23] introduced in 1979 and improved in 1989 are, however, well proven and recognized worldwide.

Note: The IEC 60534-8-4 international standard is currently being revised. The main features of the new standard are shown in [25].

When cavitation ($x_F >> x_{FZ}$) occurs, the acoustic power emitted in the octave band range of 0.5 to 8 kHz in the pipeline is obtained according to

$$L_{Wi} = 134.4 + 10 \cdot \lg \frac{W \cdot \Delta p \cdot \eta_F}{\rho_F \cdot F_L^{\,2}}$$

$$- 120 \cdot \frac{x_{FZ}^{\,0.0625} \cdot (1 - x_F)^{0.8}}{x_F^{\,x_{FZ}}} \cdot \lg \frac{1.001 - x_F}{1 - x_{FZ}} + \Delta L_F$$

$$\text{with } p \leq F_L^{\,2}(p_1 - F_F \cdot p_V) \quad (37)$$

The first row of the equation (37) represents the sound power level which is caused by the turbulent flow noise. The second row serves to calculate the sound power component which arises when the flow noise caused by the turbulence overlaps the cavitation noise resulting from the temporal static bubble collapse. Fig. 28 shows the course of the standardized sound power for standard valves with parabolic plugs ($\Delta L_F = 0$) in relation to the operating pressure ratio with x_{FZ} as a parameter. When $x_F > x_{FZ}$ applies, the noise emission rises steeply, reaches a maximum and drops back to the sound power level caused by the turbulence when $x_F = 1$.

The drop in sound power level at high pressure ratios is based, on the one hand, on the compressibility of the fluid that increases with x_F (see section on avoiding cavitation) and on the reduction of the driving force $p_2 - p_V$ when the bubble implodes (equation 10). Cavitation behavior deviating from the calculation can be taken into consideration by the valve manufacturer by specifying a valve-specific correction coefficient $\Delta L_F = f(x_F, y)$.

The spectral distribution of the internal sound power level depends on the design, pressure ratios, load and x_{FZ} value of the valve. According to VDMA 24422, the spectral distribution can be reproduced for practical application in the octave band range 0.5 to 8 kHz irrelevant of the operating condition using a noise spectrum that drops 3 dB per octave.

SAMSON AG · V74/ Dob/Zin

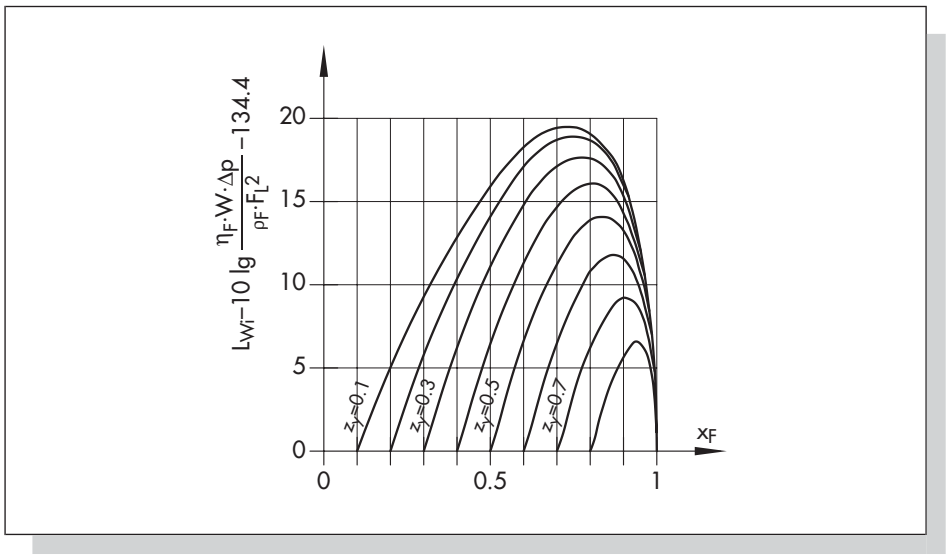

Fig. 28: Sound power for standard valves with parabolic plug ($\Delta L_F = 0$)

Several measurements performed by SAMSON resulted, however, in a sound power spectrum as shown in Fig. 29. At incipient cavitation ($x_F = x_{FZ}$), the sound power level radiated in the individual octave bands is approximately the same; the low frequencies dominate as the pressure ratio rises.

The low frequencies dominate as the pressure ratio rises

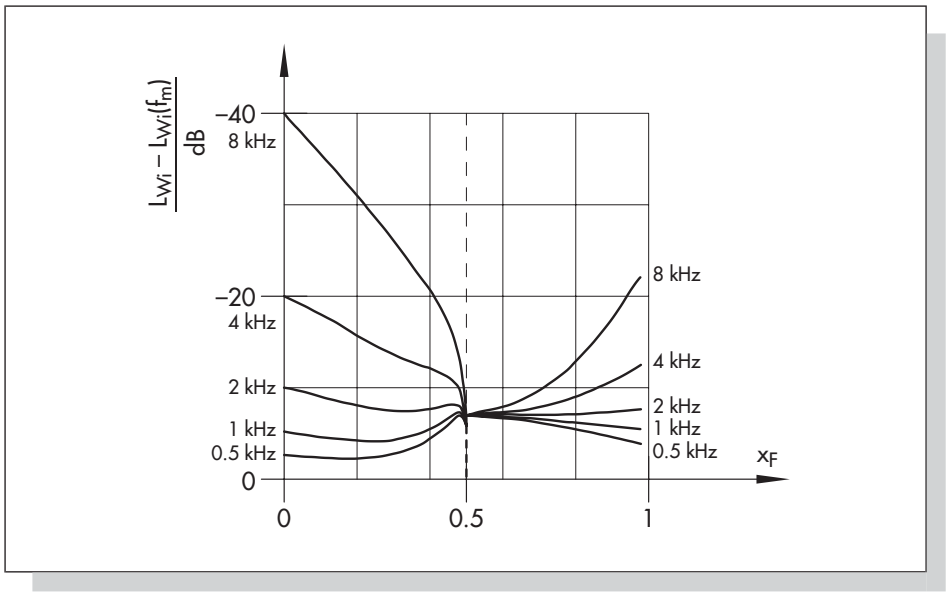

Fig. 29: Measured sound power spectrum (see also [25])

Cavitation luminescence

To conclude with, another cavitation phenomenon should be introduced which is insignificant in conjunction with control valves, but is very suitable to demonstrate again the extreme, mostly uninvestigated conditions that exist when bubbles implode: cavitation luminescence. In the cavitation zone, small flashes of light can be seen under certain conditions that have a spectral distribution from near infrared right up to the ultraviolet range. Several authors trace the light emission back to the photochemical recombination of gas molecules that have thermally dissociated when the bubbles imploded. Others believe that the flashes of light occur when the free ions recombine which arise on bubble implosion due to the mechanical load of the molecules. A further theory postulates aspherical bubbles which are surrounded by a layer of dipoles. The light appearances arise when the dipoles discharge on bubble implosion. Finally, there is the theory termed "hot spots" that assumes the gas compression linked with the bubble implosion leads to such extremely high temperatures that the gas starts to glow.

SAMSON AG · V74/ Dab/Zin

Appendix A1: List of references

[1] Ackeret, J.: Experimentelle und theoretische Untersuchungen über Hohlraumbildung im Wasser, Techn. Mechanik und Thermodynamik, Band 1, Nr. 1, Berlin, Januar 1930

[2] Becker, R.; Döring, W.: Kinetische Behandlung in übersättigten Dämpfen, in Volmer, M.: Kinetik der Phasenbildung, Verlag Steinkopf, Leipzig 1939, pages 156–165

[3] Briggs, L. J.: The Limiting Negative Pressure of Water, Journal of Applied Physics, Vol. 21, July 1950, pages 721–722

[4] Harvey, E. N.; McElroy, W. D.; Whitely, A.H.: On Cavity Formation in Water, Journal of Applied Physics, Vol. 18, Feb. 1947, pages 162–172

[5] Lehmann, A. F.; Young J.O.: Experimental Investigations of Incipient and Desinent Cavitation, Journal of Basic Engineering, June 1964, pages 275–284

[6] Jeschke, N. und Gruner, K.: Geräuschverhalten von Stellventilen, Regelungstechnische Praxis, Mai 1975

[7] DIN 45635: Geräuschmessungen an Maschinen, Blatt 50: Luftschallemission, Hüllflächenverfahren, Armaturen, August 1987

[8] Oldenziel, D. M.: Bubble Cavitation in Relation to Liquid Quality, Delft Hydraulics Laboratory, Publication No. 21, May 1979, pages 224–240

[9] Rayleigh, L.: On the Pressure Developed in a Liquid During the Collapse of a Spherical Cavity, Phil. Marg., Vol. 34, 1917, pages 94–98

APPENDIX

[10] Güth, W.: Zur Entstehung der Stoßwellen bei der Kavitation, Acustica, Vol. 6, 1956, pages 526–531

[11] Knapp, R.T.; Daily, J.; Hammit F.: Cavitation, McGraw-Hill Book Company, New York, 1970, pages 343–347

[12] Plesset, M. S.; Chapman R. S.: Collapse of an Initially Spherical Vapour Cavity in the Neighbourhood of a Solid Boundary, Journal of Fluid Mechanics, Vol. 47, Part 2, pages 283–290

[13] Lauterborn, W.: Kavitation durch Laserlicht, Acustica, Vol. 31, 1974, pages 51–78

[14] Lauterborn, W.: Jetbildung und Erosion, VDI Technologiezentrum Physikalische Technologien, Technologiefrüherkennung Band 32, Von der Kavitation zur Sonotechnologie, 2000, pages 35–36

[15] Knapp, R.T.: Recent Investigations of Cavitation and Cavitation Damage, Trans. ASME, 77, 1955, pages 1045–1054

[16] Berger, J.: Kavitationserosion und Maßnahmen zu ihrer Vermeidung in Hydraulikanlagen für HFA-Flüssigkeiten, Dissertation, TH Aachen, 1983

[17] Garcia, R.; Hammitt, F.G.: Cavitation Damage and Correlations with Material and Fluid Properties, Journal of Basic Engineering, December 1967, pages 753–763

[18] Kiesbauer, J: Stellventile bei kritischen Prozessbedingungen in Raffinerien (Control valves for critical applications in refineries), Sonderdruck „Industriearmaturen", 2001, SAMSON AG, pages 4–5

[19] Stiles, G. F.: Sizing Control Valves for Choked Conditions Due to Cavitation or Flashing, ISA Handbook of Control Valves, Instrument Society of America, 1976

APPENDIX

SAMSON AG · V74/ Dob/Zin

[20] Baumann, H. D.: The Introduction of a Critical Flow Factor for Valve Sizing, Paper presented at ISA Annual Conference, October 1962

[21] Wijngaarden, L.: Sound and Shock Waves in Bubbly Liquids, in Lauterborn, W.: Cavitation and Inhomogenities in Underwater Acoustics, Springer Series in Electrophysics 4, Springer Verlag, Berlin Heidelberg, 1980, pages 127–140

[22] Lyamshev, L. M.: On the Theory of Hydrodynamic Cavitation Noise; Soviet Physics-Acoustics, Vol. 14, No. 4, April-June 1970

[23] VDMA-Einheitsblatt 24422, Richtlinien für die Geräuschberechnung bei Regel- und Absperrarmaturen, Beuth Verlag, Berlin, Januar 1989

[24] Vnucec, D., Kiesbauer, J.: Übersicht über die Genauigkeit von Schallberechnungsnormen b. Stellgeräten (Evaluating the calculation accuracy provided by the relevant noise prediction standards for control valves), Oldenbourg Verlag, München, Germany, Heft 7, 2003

[25] Kiesbauer, J., Baumann, H.D.: "News in the prediction of hydrodynamic noise of control valves", Industriearmaturen , Vulkanverlag, Essen, Germany, Heft 3,2002

APPENDIX

Figures

FIGURES

SAMSON AG · V74/ Dab/Zin

FIGURES

NOTES

SAMSON right on quality course

Our quality assurance system,

approved by BVQI, guarantees

high-quality products and services

SAMSON AG · MESS- UND REGELTECHNIK · Weismüllerstraße 3 · 60314 Frankfurt am Main
Telefon 069 4009-0 · Telefax 069 4 009-1507 · E-Mail:samson@samson.de · Internet: http://www.samson.de

2003/11 · I351 EN